Cellular and Molecular Life Sciences (2021) 78:6119–6141
https://doi.org/10.1007/s00018-021-03904-9

REVIEW

Ultrasonic technologies in imaging and drug delivery

Yi-Ju Ho[1] · Chih-Chung Huang[2,3] · Ching-Hsiang Fan[2,3] · Hao-Li Liu[4] · Chih-Kuang Yeh[1]

Received: 9 May 2021 / Revised: 13 July 2021 / Accepted: 19 July 2021 / Published online: 23 July 2021

Abstract

Ultrasonic technologies show great promise for diagnostic imaging and drug delivery in theranostic applications. The development of functional and molecular ultrasound imaging is based on the technical breakthrough of high frame–rate ultrasound. The evolution of shear wave elastography, high-frequency ultrasound imaging, ultrasound contrast imaging, and super-resolution blood flow imaging are described in this review. Recently, the therapeutic potential of the interaction of ultrasound with microbubble cavitation or droplet vaporization has become recognized. Microbubbles and phase-change droplets not only provide effective contrast media, but also show great therapeutic potential. Interaction with ultrasound induces unique and distinguishable biophysical features in microbubbles and droplets that promote drug loading and delivery. In particular, this approach demonstrates potential for central nervous system applications. Here, we systemically review the technological developments of theranostic ultrasound including novel ultrasound imaging techniques, the synergetic use of ultrasound with microbubbles and droplets, and microbubble/droplet drug-loading strategies for anticancer applications and disease modulation. These advancements have transformed ultrasound from a purely diagnostic utility into a promising theranostic tool.

Keywords Diagnostic ultrasound imaging · Ultrasound contrast agent · Blood–brain barrier opening · Local drug release · Tumor therapy · Neuromodulation

Introduction

Ultrasound, defined as a frequency of sound wave greater than 20 kHz, has various applications including water depuration, navigation, and medicine [1]. In the clinic, ultrasound is a frontline tool for monitoring patient health or detection of disease. The many benefits of ultrasound, including its portability and the ability to provide non-invasive, real-time imaging with deep penetration and using non-ionizing radiation, have valuable potential for functional and molecular imaging [2]. Microbubbles (MBs) show good contrast enhancement on ultrasound imaging and are recognized as ultrasound contrast agents [3]. These micro-sized bubbles can flow through the entire blood circulation via intravenous (IV) injection to provide information on blood perfusion in organs. Recent technological advances and improvements in computer hardware have increased the calculation capacity for complex imaging processes. The breakthrough in frame rate in ultrasound imaging promoted the emergence of ultrafast ultrasound imaging, in turn leading to the development of a variety of novel imaging processes for functional ultrasound imaging [4]. The development and utilization of ultrasound contrast media has further increased the diagnostic capability of medical ultrasound.

Recently, it has become apparent that many of these contrast media also exhibit biophysical effects in combination with ultrasound that can be exploited for therapeutic purposes. The structure of MBs not only enhances image contrast for diagnosis but also provides a suitable vehicle for

Yi-Ju Ho and Chih-Chung Huang both are contributed equally.

✉ Hao-Li Liu
hlliu@ntu.edu.tw

✉ Chih-Kuang Yeh
ckyeh@mx.nthu.edu.tw

1 Department of Biomedical Engineering and Environmental Sciences, National Tsing Hua University, Hsinchu, Taiwan

2 Department of Biomedical Engineering, National Cheng Kung University, Tainan, Taiwan

3 Medical Device Innovation Center, National Cheng Kung University, Tainan, Taiwan

4 Department of Electrical Engineering, National Taiwan University, Taipei, Taiwan

loading cargo such as drugs for therapy. When cargo-loaded MBs are stimulated by ultrasound, the cavitation behavior of MBs locally releases the cargo and enhances cell/vessel permeability, thus promoting cargo delivery [5, 6]. MB cavitation can also open the blood–brain barrier (BBB) to overcome the limitation of drug delivery in the brain [7]. The safety of BBB opening induced by MB cavitation has been demonstrated and this technique is now being transferred into the clinic [8]. Moreover, phase-change droplets are converted into bubbles after ultrasound-triggered vaporization, providing another source of ultrasound contrast agent [9]. Droplets composed of a lipid shell and liquid core can easily be made nano-sized and provide a longer in vivo lifetime for therapeutic applications [10]. The mechanism of local drug release and the bioeffects induced by droplet vaporization are similar to those of MB cavitation [11, 12]. Notably, the therapeutic effects of ultrasound-stimulated MBs or droplets can be combined with real-time ultrasound contrast imaging to provide various theranostic applications.

This review provides an overview of recent developments of ultrasonic technologies in imaging and drug delivery. The first section describes the evolution of ultrasound imaging and novel functional imaging processes such as ultrafast ultrasound imaging, shear wave elastography, high frequency ultrasound imaging, ultrasound contrast imaging, and super-resolution blood flow imaging. The second section introduces therapeutic applications of MBs, including cargo loading, cellular bioeffects, and local drug delivery. The pharmacokinetics of cargo-loaded MBs are compared with those of mixing cargo with MBs with regard to the efficiency of local drug delivery. The third section focuses on applications of MBs in the central nervous system (CNS) and describes safety, therapy for tumors and neurodegenerative diseases, neuromodulation, and immune responses in the brain. The development of clinical trials using MBs for BBB opening is also presented. The final section covers development of phase-change droplets. The acoustic features of droplets are introduced to illustrate the diagnostic and therapeutic applications and the regulation of droplet vaporization and condensation is discussed to show the reproducibility of drug release and contrast enhancement in ultrasound imaging. Finally, some limitations and future developments of ultrasonic technologies in imaging and drug delivery are considered.

Ultrasound imaging

Diagnostic ultrasound imaging

Medical ultrasound imaging has been used widely in many clinical applications, including obstetrics and gynecology, cardiology, hepatobiliary disease, and gastroenterology, due to its portability and the ability to perform non-invasive, real-time imaging without exposure to ionizing radiation [13]. Figure 1a shows a basic schematic diagram of the modern medical ultrasound imaging system, including the ultrasound transducer, pulser-receiver front end, beamformer, analog-to-digital converter (ADC), and personal computer–based software for imaging processing [14]. The ultrasound transducer is made of piezoelectric material, which usually has a center frequency around 3.5–15 MHz

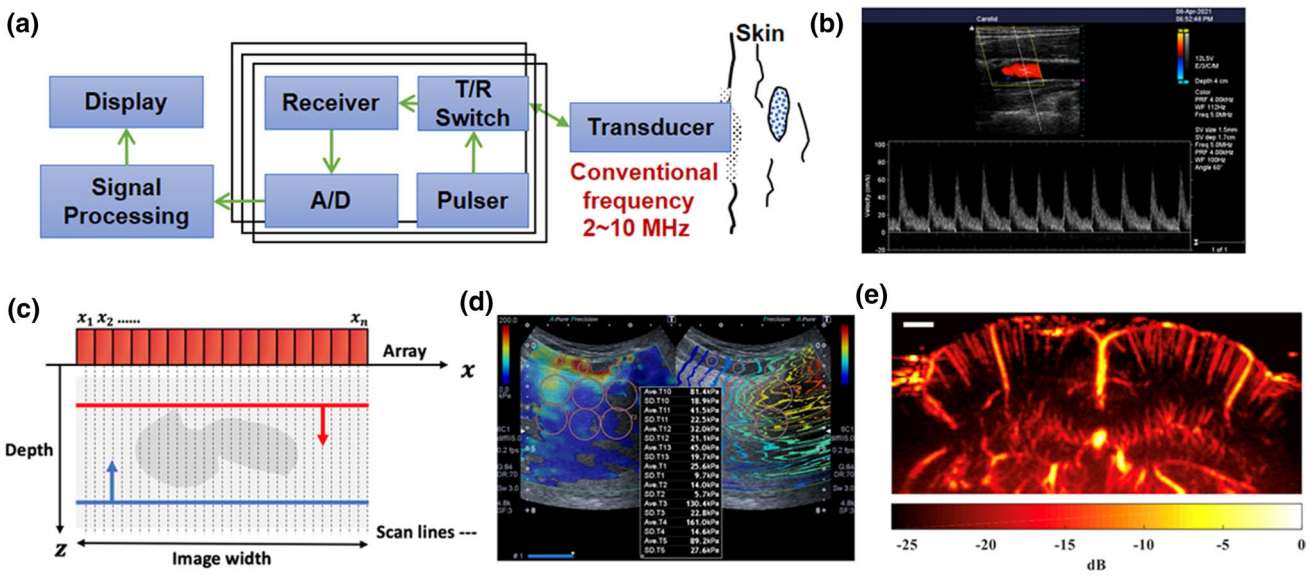

Fig. 1 **a** Basic schematic diagram of the modern medical ultrasound imaging system, **b** a typical ultrasound Doppler mode image, **c** the principle of ultrasound plane wave imaging, **d** typical ultrasound shear wave elastography, and **e** super-resolution blood flow imaging of mouse brain [65]

in most clinical applications. Unlike X-ray imaging or radionuclide emission tomography, which use a transmission method for imaging, medical ultrasound imaging is based on a "pulse-echo" approach. The ultrasound wave generated by the transducer propagates in soft tissues and the echo signals are obtained as a result of mismatch of acoustic impedance at the tissue interface. After the echoes are received by the same transducer elements, the signals are first amplified by the front-end hardware and subsequently fed to the software for imaging processing via the ADC. The beamformer plays an important role in focusing the ultrasound beam to provide better image quality. Since the array transducer is used in most modern ultrasound machines, the electronic line-by-line scan is performed by the beamformer for two-dimensional (2D) imaging. Finally, several image modes are displayed for diagnosis, such as B-mode (brightness), M-mode (motion), and Doppler mode for blood flow measurements [15], as shown in Fig. 1b.

The received echo, the so-called A-line signal, represents the backscattering signal as a function of time of flight along the ultrasound beam. The amplitudes of A-line signals are then transferred to the brightness or gray scale across all scanning lines to form the 2D B-mode image, which is the fundamental principle of the ultrasound gray level image. Currently, a modern ultrasound machine can provide B-mode images at more than 30 frames per second (fps) to allow imaging of organ motion. In M-mode imaging, which is frequently used to monitor mitral valve prolapse in echocardiography, only one A-line signal along the time axis is selected for gray scale imaging [16–18]. In addition to anatomical information on organs, ultrasound also provides blood flow measurements based on the Doppler effect. Three Doppler modes are commonly used in ultrasound: Doppler sonography (continuous wave and pulsed wave), color Doppler imaging, and power Doppler imaging. Doppler sonography provides the variation of flow velocity in a specific vessel along the time axis. Color Doppler imaging also displays blood flow information (velocity and direction) on the B-mode image, the so-called duplex scanner, in real time. The color encoded on the B-mode not only represents the value of flow velocity but also the flow direction; the red and blue colors indicate flow toward and away from the transducer, respectively. Power Doppler is also useful for clinical diagnosis, particularly for perfusion imaging. Since the "power" only considers the energy of backscattering signals from blood cells, power Doppler exhibits a high sensitivity in detecting the smaller vessels [2, 19].

Ultrafast ultrasound imaging

As mentioned above, the frame rate of current ultrasound imaging machines is approximately 30–100 fps, which is sufficient for most clinical applications including echocardiography. However, high frame rate ultrasound imaging, so-called ultrafast ultrasound imaging, has recently been achieved with improvements of ultrasound hardware. One major advantage of ultrafast ultrasound imaging is that it converts the ultrasound image into a "high speed camera", in which any movement of an object in the view of the ultrasound exhibits "slow motion". Another breakthrough in ultrasound hardware is the graphical processing unit (GUP) that provides parallel computing ability, allowing the hardware to process a huge amount of ultrasound data simultaneously [20]. Since the conventional ultrasound machine uses the beamformer to generate a focusing beam for line-by-line scanning of the object, time is required for transmission and receiving the backscatter signals during scanning. For example, assuming that the sound velocity is about 1540 m/s, the imaging depth is 5 cm, and 256 scanning lines are used for imaging, a frame rate of 60 fps can be achieved with a conventional ultrasound machine [4].

Several approaches have been proposed in order to achieve high frame rate ultrasound imaging, such as the time-reversal approach [21] and nondiffracting beams approach [22]. Currently, use of plane wave imaging is the standard for ultrafast ultrasound imaging [20, 23]. Unlike the conventional ultrasound machine, which uses a line-by-line scanning approach, the plane wave is generated by firing all the elements of an array transducer simultaneously in one shot as shown in Fig. 1c. As a result, the frame rate of plane wave imaging can be > 10 k fps. However, although use of the single plane wave for ultrasound imaging definitely increases the frame rate, the image quality is reduced due to the inability to focus. To overcome this problem, coherent plane wave compounding imaging has been proposed to improve the image quality of plane wave imaging [23, 24]. Several plane waves with different tilted angles are transmitted to the object and the received images with different angles are summed coherently to form a high-quality image. As more tilted plane waves are applied the image quality is improved; however, increasing the number of tilted plane waves also reduces the frame rate of imaging, resulting in a trade-off between image quality and frame rate in coherent plane wave compounding imaging [20]. Nonetheless, a frame rate of several thousand fps can currently be achieved with acceptable image quality. With the emergence of ultrafast ultrasound imaging, several new applications of ultrasound imaging have been proposed such as shear wave elastography, super resolution blood flow imaging, and ultrasound contrast imaging, which will be discussed in the following sections.

Ultrasound elastography

As the mechanical properties of soft tissue are often altered in the disease state, measurement of tissue viscoelasticity, or

elastography, is also used in diagnostic ultrasound imaging. Measurement of tissue stiffness is an important index for clinical diagnosis; for example, a tumor is typically stiffer than the surrounding normal tissues. Ultrasound imaging currently plays an important role in assessing tissue stiffness in clinical diagnosis. Compressional ultrasound elastography was first proposed by Dr. Ophir in 1991 for breast cancer diagnosis [25]. In this approach, the transducer is used to compress the human body directly; since the stiffer tissue has a smaller displacement compared to its surrounding normal tissues the displacement is measured by ultrasound image via cross-correlation algorithm and the strains of different tissues are displayed to present the stiffness distribution. However, compressional ultrasound elastography only provides the relative stiffness and its quality is highly dependent on the skill of the operator. In addition, ultrasound wave transfers momentum to the medium producing an acoustic radiation force, which induces medium movement in the wave propagation direction [26]. Acoustic radiation force impulse (ARFI) imaging was subsequently proposed for "remote palpation" of tissue for elastography [27, 28]. In ARFI imaging, a high-intensity long pulse ultrasound wave generated by an array transducer is applied to push the tissue and the subsequent tissue displacement is detected by ultrasound imaging pulses via the same transducer. Since these displacements are directly correlated with localized variations of tissue stiffness properties, the relative stiffness is displayed for elastography. ARFI imaging has been used in basic research and for several clinical applications, such as determining malignant lesions of breast [29], manipulating the vitreous humor of the eye [30], and for vibro-acoustography [31]. In addition, ARFI imaging has been applied for blood clot assessment [32], monitoring chemical and thermal ablations [33], and corneal sclerosis [34]. Again, as ARFI imaging only provides the relative stiffness of soft tissue a quantitative imaging method is needed to obtain the elastic modulus of tissue.

Recently, shear wave imaging has become the standard of ultrasound elastography [35–37]. Since the shear wave propagation velocity (c) in tissue is directly related to the elastic modulus (E) of medium based on $E = 3\,\rho c^2$ (ρ=tissue density), the quantitative stiffness distribution is obtained for 2D elastography [38]. Because the shear wave velocity is quite fast, ultrafast ultrasound imaging is needed to track the shear wave. In shear wave imaging an ARFI is generated by an array transducer to vibrate the tissue and create the shear wave propagation, and then the ultrafast plane wave imaging is fired to track the wave velocity. A region with a faster shear wave velocity indicates stiffer tissue, as shown in Fig. 1d. Shear wave imaging is independent of the skills of the operator and provides a quantitative elastic modulus of tissue. Elastography with most modern clinical ultrasound machines is based on shear wave imaging, including shear wave elastography of breast [39, 40], liver [41, 42], thyroid [43], skeletal muscle [44], eye [45–47], blood clot [48], and intravascular ultrasound [49].

High-frequency ultrasound imaging

The operational frequency of the conventional ultrasound imaging machine is around 2–18 MHz, which provides sufficient image resolution with an appropriate imaging depth for clinical applications. However, the spatial resolution of ultrasound imaging can be improved by increasing the operational frequency, for example, 50 MHz ultrasound imaging provides lateral and axial resolution of 100 and 20 μm, respectively [2]. Due to the nature of high attenuation for high frequency ultrasound imaging (HFUS, > 30 MHz), the penetration depth would be limited to within 10 mm. HFUS has been used widely in many preclinical and clinical applications. The single element transducer imaging system was first proposed using a mechanical scanning approach, so-called ultrasonic biomicroscopy (UBM) [50, 51]. UBM provides the B-mode, M-mode, and Doppler mode in real-time but the frame rate is not as high due to the mechanical scanning [52–54]. The basic principle of UBM is similar to that of the diagnostic ultrasound imaging system. Since a single-element transducer is used the operational frequency could be in the GHz range but is around 30–50 MHz for most biomedical applications [55, 56]. Currently, the HFUS array transducer is commercially available at a center frequency up to 50 MHz (Vevo 3100), providing a greatly increased imaging frame rate with convenient operation for the user. Nevertheless, HFUS imaging has been used widely in small animal imaging for gene research [57], cancer studies [58], and various preclinical studies [59, 60], and the HFUS imaging machine has been approved by the U.S. Food and Drug Administration for diagnosis in humans. More recently, ultra-fast HFUS imaging combining a high frequency array transducer with programmable ultrasound imaging has been proposed [24]. Therefore, high-resolution ultrasound elastography and super-resolution blood flow imaging are currently available for biomedical applications [61–66].

Contrast imaging: perfusion and super-resolution imaging

Since the ultrasound backscatter signals from the blood are weaker than those from other tissues, the lumen on the B-mode image exhibits a lower echogenic region (dark region). Usually, the small vessels cannot obviously be identified on the gray scale ultrasound image; however, the echoes from blood can be enhanced by injection of an ultrasound contrast agent such as MBs into the vessel. This contrast-enhanced ultrasound imaging (CEUS) is useful for monitoring the blood flow conditions and evaluating perfusion, particularly for heart

and liver applications. Currently, several ultrasound contrast agents are available for clinical use, such as Levovist (Schering AG), Albunex (Mallinckrodt Pharmaceuticals), Sonazoid (Amersham Health Inc.), SonoVue (Bracco Imaging SpA.), Definity (Bristol-Myers Squibb), and Optison (Amersham Health Inc.) [3, 67]. MBs respond to ultrasound by oscillating radially, exhibiting linear or nonlinear behavior depending on the ultrasound frequency and acoustic pressure, as illustrated by the mechanical index (MI). Harmonic imaging is the mainstay of CEUS in modern ultrasound machines [2]. Perfusion is measured by calculating the "time–intensity" curve from the flowing MBs at a specific region on the image [68]. The "wash-in" and "wash-out" times and other parameters from the time-intensity curve are then obtained to evaluate the perfusion of blood supply. Currently, CEUS has been used widely for applications in the liver (nodular hyperplasia, gallbladder carcinoma, malignant portal vein thrombosis) and the heart (intracardiac thrombus, myocardial perfusion, vessel wall irregularities, and intraplaque neovascularization within carotid stenosis) [69, 70].

More recently, interest in contrast imaging for blood flow imaging has focused on so-called super-resolution blood imaging as a result of the development of ultrafast ultrasound imaging [71]. Ultrafast ultrasound imaging captures more sampling points of the backscatter signals from blood compared to conventional Doppler imaging and therefore provides sufficient signal length for calculating the Doppler shift, which increases the sensitivity of blood detection. The microcirculation is then observed using ultrafast ultrasound imaging. This approach of functional ultrasound imaging has recently been used in many small animal and human brain research studies [72]. The resolution of blood flow in ultrafast ultrasound imaging can be increased by injecting the MBs into vessels, so-called super-resolution ultrasound localization microscopy (ULM) [73]. ULM was inspired by super-resolution imaging in optical microscopy. In ULM, the flowing MBs are detected by ultrafast ultrasound imaging and the point-spread function of the ultrasound system is subsequently applied on the bubble echo signal to provide the precise localization of the isolated bubbles from the super-resolution image. The bubble locations are tracked by high frame imaging and the vascular structure is mapped by accumulating the trajectory of bubble locations [74]. Currently, ULM is not available in clinical ultrasound machines but many studies have applied it in preclinical and clinical research settings for cancer, brain, kidney (Fig. 1e), skin, and cardiovascular studies [65, 71].

Microbubbles

Drug-loaded MBs

Microbubbles are not only useful as contrast agents in ultrasound imaging but also have the ability to carry therapeutics. The strategies for loading MBs with therapeutics will be summarized in this section. The physical structure of MBs makes them suitable to serve as vehicles for therapeutic cargos (drugs, genes, nanoparticles, or therapeutic gas) through incorporation into the MB shell, by dissolving them in an oil layer between the MB shell and core, or by attaching larger molecules or nanoparticles onto the MB shell [38, 75–77]. The earliest design of cargo-loaded MBs was reported by Unger et al. in 1998 [78]. These cargo-loaded MBs were produced via mechanical agitation of a perfluorobutane gas paclitaxel-containing emulsion and liposomes. The results showed that the lipid shell of MBs decreased the direct exposure of paclitaxel to plasma, thus reducing its systemic toxicity in vivo. In addition, the shell of the MBs can be modified with disease-associated biomarkers to further improve treatment localization for specific molecular theranostic purposes or targeted therapy [79, 80].

The strategy adopted for MBs carrying cargo mainly depends on the nature of the cargo. For instance, hydrophobic cargos could be embedded between the lipid shell and the gas core, whereas hydrophilic cargos may be attached to the outer surface either directly [81] or packaged within liposomes [76]. In previous studies, cargo-loaded MBs could be produced by direct mixing with the cargo during MB preparation but the payload is limited and varies depending on the property of the drug (hydrophilic or hydrophobic). To address this issue, preparation of an additional oil layer between the lipid shell and gas core might help to trap cargo [78], although higher ultrasound energy would be necessary to activate the release of loaded cargo from this framework [82]. Cargo could be attached to the outer shell surface of MBs through covalent binding (e.g., streptavidin–biotin interaction) or non-covalent binding. Through electrostatic interaction, the lipid shell of MBs with a positively charged lipid component could function as a carrier of negatively charged nucleic acids (e.g., pDNA, siRNA, mRNA) [83]. A multilayered positively charged poly-L-lysine and nucleic acids structure has been proposed to further improve the payload of nucleic acid while maintaining high MB stability [83].

It is possible to directly use a low molecular weight enzyme such as lysozyme as the shell of MBs [84, 85]. Through dispersion of a gas phase in the protein solution, the gas core would be stabilized within the protein-linked skeleton. Such enzyme-shelled MBs could be further

coated and functionalized with a number of biomacromolecules (proteins, polysaccharides, or nucleic acids) [84]. The cargos can be pre-encapsulated into carriers (i.e., micelles, microspheres, or liposomes) and then conjugated on the surface of MBs, for example through thiol-sulfhydryl group linkage or avidin–biotin interaction [86, 87]. Such MB complexes have a higher drug payload than other strategies and can encapsulate drugs of different polarity. MBs are also being investigated as a gas carrier for delivery of therapeutic gases, including oxygen for hypoxia, drug penetration, and vasculature normalization in tumors or nitric oxide for cardiovascular disease [88–91].

Cellular drug uptake/gene transfection under MB cavitation

The viscoelastic lipid shell and compressible gas core allows the MBs to volumetrically oscillate, a process termed cavitation, in response to the rarefaction and compression portions of the ultrasound wave, potentially providing a unique opportunity for drug delivery. The interactions between cargo-loaded MBs and cells for drug delivery will be discussed in this section. Upon ultrasound sonication the cargo-loaded MBs locally release their cargo while the concurrent MB cavitation improves uptake of the released cargo. Several mechanisms of cargo release from MBs have been identified. For example, MBs can be converted into 200–500 nm drug-containing fragments by ultrasound [92, 93]. Alternatively, the oscillation of MBs can release shell fragments (called lipid shedding), and these fragments can be further transported via acoustic microstreaming [94]; the occurrence and distance of shedding can be increased by applying higher acoustic pressures. The cargo-loaded MBs may also result in direct deposition of the cargo onto the cell membrane, potentially allowing delivery of a large amount of drug or gene to the targeted cells [95–97].

The micrometer scale of MBs enables generation of several microscale mechanical responses in an ultrasound field and therefore the bioeffects of MB cavitation can be greatly focused at the cellular level. The oscillating MBs also elicit microscale shear forces that can induce physiological changes or tear the lipid membrane of cells, temporarily permeabilizing the cellular membrane and enhancing cellular endocytosis uptake [98–100]. To date, four biological phenomena have been observed: sonoporation, stimulated endocytosis, opening of cell–cell contacts, and sonoprinting [5, 101–103].

Sonoporation involves the generation of reversible pores on the cellular membrane as a result of mechanical agitation from persistent, low-amplitude MB oscillations (commonly termed stable cavitation) or violent MB collapse (commonly termed inertial cavitation) close to the cell membrane [104]. Generally, the size (a few nm to hundreds of nm) and resealing time (within seconds) of pores produced by stable cavitation are lower than those of pores caused by inertial cavitation (hundreds of nm to μm; up to 1 min) [105–107]. The pores can pass through not only the apical cell membrane layer but also the basal cell membrane layer [99]. In addition to poration of a single cell, sonoporation can also disrupt cell–cell contacts and produce intercellular gaps between adjacent confluent human umbilical vein endothelial cell monolayers with a resealing time of 30–60 min [104].

Previous studies observed that ultrasound with MBs would temporarily activate a cellular endocytosis effect for internalization of substances ranging from hundreds of nm to μm, including clathrin-mediated endocytosis (~ 200 nm), caveolae-mediated endocytosis (~ 500 nm), and micropinocytosis (> 1000 nm) [108]. Observation by electron microscopy showed the appearance of caveolar endocytic vesicles after ultrasound with MB treatment [109]. To date, studies have reported two mechanisms by which ultrasound and MBs might stimulate cellular endocytosis [110]: the tension of the cell membrane might be modulated by MB-induced mechanical force, or endocytic uptake of fluid-phase subjects might be promoted by the microstreaming and shear stress [100, 111].

Sonoprinting is a newly characterized mechanism that only occurs in cargo-loaded MBs. Studies showed that the cargos were directly transported from the MBs to patches on the cellular membrane and then internalized within 1 h [95–97]. Via this route, the lipid components of the cargo are fused or exchanged with the cell membrane, achieving cytosolic delivery without endosomal degradation. Initiation of sonoprinting requires high acoustic pressure (> 300 kPa) and long pulses (> 100 cycles) under an acoustic frequency of 1 MHz [96]. It was recently reported that sonoprinting could occur not only in 2D cell monolayers but also in free-floating 3D tumor spheroids, indicating wide applications of this approach [97]. Ho et al. reported that in the scenario of cargo-loaded MBs attached on the cell membrane, stable cavitation of MBs could transfer tenfold more cargo to cells compared with inertial cavitation, without lethal cellular damage [112].

Enhanced vascular permeability for local drug delivery

Permeabilization of endothelial vasculature can also be accomplished via MB cavitation effects, and the in vivo bioeffects of MBs cavitation on vessels and their applications for disease treatments are discussed in this section. Recent studies have observed four temporary physiological changes of vessels stimulated by ultrasound and MBs. First, the gap-junction distance between endothelial cells can be expanded during MB oscillation, thereby allowing the circulating

agents to extravasate [104]. Second, the quick vibration of MBs also produces local microstreaming to stimulate nearby vascular endothelium. This MB-generated streaming is at least 25-fold faster than the blood flow, and, therefore, disturbs the integrity of the endothelial lining [104, 113, 114]. Third, the cell membrane potentials are changed during MB vibration, probably eliciting endocytotic activity and intracellular pathways. Fourth, the MBs may be squeezed through the endothelium and tunnel through soft tissue during ultrasound sonication [115, 116], potentially resulting in deposition of drugs beyond the vasculature.

MB and free drug physical mixtures

The most common application of MB-induced vascular permeabilization for enhanced drug delivery involves simple physical mixtures of MBs and free drugs (Table 1). Upon the trigger of ultrasound, the free drug can selectively extravasate in the ultrasound-sonicated area via the abovementioned routes. There have been a number of efforts to deliver immune substances for elimination of solid tumors using this procedure: Heath et al. reported that intracellular uptake of a monoclonal antibody (cetuximab) could be improved by 30% in a head and neck squamous cell carcinoma model [117]; pDNA encoding a cytokine (interleukin-27, interleukin-12) could be successfully delivered in mice models of prostate tumor (RM1, TRAMP-C1 and TRAMP-C2), hepatocellular carcinoma, or OV-HM tumor [118–120]; and tumor-associated antigen (ovalbumin) could be transferred into dendritic cells by combination treatment of bubble liposomes, ultrasound, and antigen [121, 122]. The feasibility of delivering chemotherapeutic drugs for MB-assisted chemotherapy has also been confirmed in cell culture systems, animal studies, and even in clinical trials (for example, breast cancer, pancreatic cancer, colorectal cancer, radioembolization of liver cancer, and liver cancer) [123–126]. In one phase I clinical trial, tumor size reduction was observed in five patients, and median survival increased from 8.9 months to 17.6 months without additional side effects [125].

For application in thrombolysis, the penetration of thrombolytic drugs into the blood clot can be enhanced by ultrasound with MBs, reducing clot size by 39–69% and thrombolysis time in stroke patients [127]. Antibiotic resistance induced by bacterial infection can also be addressed using MB – drug physical mixtures. The protective barrier of biofilms can be disrupted by MB cavitation to enhance the delivery of antibiotic, a process termed sonobactericide [128, 129]. A combination of MBs, oxacillin (antibiotic), and recombinant tissue plasminogen activator (thrombolytic) as a treatment for infective endocarditis reduced clot size by $99.3 \pm 1.7\%$ [130]. In a rabbit model with an implanted biofilm-containing catheter, the synergistic effect of ultrasound-mediated MBs combined with vancomycin decreased biofilm viability twofold compared with the untreated group [131].

Cargo-loaded MBs

The limitations of a mixture of free drug and MBs include poor pharmacokinetics of free drugs, lack of targeting, and easy degradation of drugs within the in vivo circulation. To overcome these issues and expand the medical applications, several efforts have been made to develop cargo-loaded MBs (Table 1). Using microscopic imaging and fluorescent dyes, ultrasound-sonicated MBs were shown to significantly transfer their cargo onto excised rat cecum and living mouse dorsal vessels, suggesting the possibility of vascular local delivery in vivo [82, 112]. In one study using paclitaxel

Table 1 Comparison of MB-assisted drug delivery systems

Parameter	MB and free drug (Physical mixtures)	Cargo-loaded MBs
Application	Tumor therapy [123–126]	Tumor therapy [134, 135]
	Immune therapy [117–122]	Immune therapy [136]
	Thrombolysis [127]	Neointimal hyperplasia inhibition [132, 133]
	Antibacterial infection [128–131]	Hair growth recovery [87]
		Antibacterial infection [85, 137]
		Vaccine therapy [138–140]
Preparation	Easy [123–126]	Dependent on cargo property [76, 78, 81, 83–91]
Activation step	Injected as ready to use [128, 129]	Injected as ready to use [87, 134, 135]
	Drug administration following MBs injection [113–116]	
Activation time	Few seconds to few minutes [104–107]	Immediately [95–97]
Advantages	Easy preparation [123–126]	Reduced systemic cytotoxicity of drug [78]
		Prolonged drug lifetime within circulation [141–143]
Disadvantages	Direct drug exposure in blood circulation [245]	Poor stability, payload highly dependent on cargo property, risk of drug leakage [246]

loaded into MBs, neointimal hyperplasia in the rabbit iliac balloon injury model was inhibited by drug released from the MBs [132]. In a similar study, Kilroy et al. showed a 60% decrease in neointima formation by rapamycin-loaded MBs in a swine model [133]. As an antitumor approach, a Rose Bengal sonosensitizer has been covalently attached to the shell of MBs and used to produce a high level of reactive oxygen species, resulting in cytotoxicity to cancer cells [134, 135]. In addition, conjugation of interleukin 8 monoclonal antibody allowed the MBs to selectively adhere and neutralize atherosclerosis plaques, alleviating the interleukin 8–related inflammation response [136].

The applications of MBs decorated with cargo-containing liposomes have been explored by several groups. In 2020, Ryu et al. proposed a MB-nanoliposomal complex as a Cas9/sgRNA riboprotein complex carrier. They concluded that the production of SRD5A2 protein could be suppressed by MB-assisted CRISPR-based genomic editing, resulting in recovery of hair growth in mouse skin [87]. Horsley et al. demonstrated that MBs loaded with gentamicin-liposomes could efficiently transfer drugs to urothelial cells for treatment of urinary tract infection [137]. Liao et al. applied lysozyme-shelled MBs and ultrasound to inhibit *P. acnes*-induced inflammatory skin diseases [85]. In the application of DNA vaccine therapy, Un et al. reported increased cytotoxic T lymphocyte activities and secretion of Th1 cytokines (i.e., interferon-γ, tumor necrosis factor-α) after treatment with MB lipoplexes loaded with pDNA encoding melanoma antigen (i.e., gp 100, tyrosinase-related protein 2) combined with ultrasound [138]. In E.G7-OVA cell and EL4 cell tumor models, the tumor volume shrank 4.5-fold and the antitumor effects were maintained for at least 80 days after treatment with pDNA-lipoplex–loaded MBs with ultrasound [139]. Dewitte et al. reported that MBs loaded with TriMix mRNA and antigen can stimulate strong immune responses in vivo, producing a decrease of tumor outgrowth, an obvious increase in survival, and antigen-specific immunological memory [140].

Another advantage of cargo-loaded MBs is that the shell of the MBs can prevent direct exposure of chemotherapeutic drugs to blood circulation, thus reducing their systemic toxicity. One study reported an obvious reduction in systemic toxicity for animals treated with paclitaxel-loaded MBs [78]. In addition, the MBs can prolong the half-life of the therapeutic substances (especially nucleic acids) during circulation by preventing their degradation and clearance [141–143]. The efficacy of cargo-loaded MBs could be further enhanced by functionalization with disease-associated ligands, such as LHRHa, Lyp-1, and CD105 antibody [144–146]. The local drug concentration and MB-generated mechanical bioeffects would be increased by concentrating MBs at a specific area, thus reducing the dosage required to yield a significant response. In addition, the occurrence of off-target effects would potentially be avoided, increasing the safety of this treatment. Recently, drug-loaded MBs tethered with magnetic nanoparticles have been proposed as a means to magnetically aggregate and manipulate the MBs at the desired site with spatial resolution of several millimeters [147–149]. This strategy can potentially circumvent the immune issues currently associated with antibody-linked MBs.

Application of ultrasound with MBs in the CNS

Development of CNS-purposed therapeutic ultrasound has continued since the Fry brothers first investigated the focused ultrasound (FUS) apparatus for CNS application in the 1950s. In the early 2000s there was an initial attempt to combine the use of MBs with therapeutic ultrasound. Since the MBs locally amplify acoustic emission to the capillary lumen, the induced bioeffect is readily observed with acoustic exposure level up to two orders of magnitude lower than in the absence of MBs. With a burst-type ultrasound exposure and under concurrent intravenous administration of MB, one of the most noticeable effects in capillaries is the induction of tight junctional disruption. Since FUS has many unique advantages including transcranial noninvasiveness, efficient targeting to deep-seated brain regions, and tight junctional disruption transients, its use in the presence of MBs has become a novel and useful tool to target "opening" of the BBB and has been used in many innovative applications (Fig. 2). In the following section we review BBB opening technology, including the induced biological impact, potential therapeutic applications, the accompanying neuromodulation, and the immunomodulation effect.

MB-enhanced ultrasound: Histological impact

Hynynen et al. first demonstrated that ultrasound exposure in the presence of MBs can transiently permeate the CNS capillary (so-called BBB opening) and the pressure level required to disrupt the BBB has been confirmed to be significantly reduced compared with ultrasound exposure without MBs (two orders of magnitude reduction in acoustic intensity) [150]. An early study in the development of MB-ultrasound–induced BBB opening tested the histological effect of a wide range of ultrasound exposure levels. For pressure levels ≥ 6.3 MPa (1.5-MHz, 10-μs pulse length, duty cycle 1%), apparent vascular wall damage, tissue necrosis, ischemia, and apoptosis were observed [151]. McDannold et al. further examined a relatively narrow acoustic exposure range (1.63 MHz, 100 ms pulse length, duty cycle 10%, 0.7–1.0 MPa) with additional testing of whether a delayed effect exists for MB-ultrasound BBB

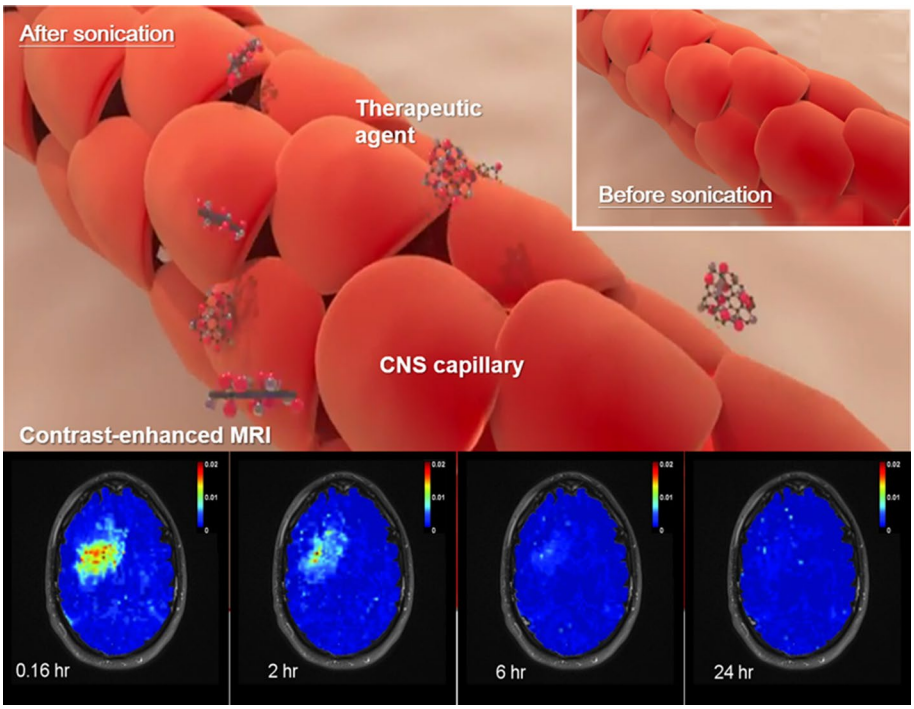

Fig. 2 Conceptual diagram showing the use of FUS exposure in the presence of MBs to open the BBB in CNS

opening. With a significant reduction in exposure level (0.7 MPa), the major observation was small-scale red blood cell extravasations while the apoptosis and ischemia became minimal [152]. In addition to histological examination, T2*-weighted magnetic resonance imaging (MRI, or MR susceptibility weighted imaging) has been used to detect potential hemorrhage accompanying the MB-ultrasound BBB opening process [153, 154].

Brain tumor treatment

MB-ultrasound BBB opening has been reported to enhance the delivery of small molecular anticancer drugs including carmustine, temozolomide, irinotecan, doxorubicin (Dox), and paclitaxel for brain tumor treatment [155–160]. For therapeutic drugs that cannot efficiently penetrate into the brain such as irinotecan (the concentration of irinotecan within the intact brain was reported to be as low as a 2% tissue/plasma ratio), the concentration can be increased by 178% after MB-ultrasound BBB opening [159]. Paclitaxel also shows limited therapeutic benefit in brain tumors due to the BBB effect. FUS-BBB opening facilitates the penetration of paclitaxel into the brain by approximately three- to fivefold using various drug formulations [160]. Larger anticancer agents such as liposomal Dox [161–163], carboplatin [164], and interleukin-12 [165] can also be successfully delivered into the brain.

In addition to delivery of anticancer chemotherapeutic agents, MB-ultrasound BBB opening has been shown to successfully deliver therapeutic proteins or monoclonal antibodies for brain tumor treatment. BBB opening can be used to deliver large molecular therapeutic monoclonal antibodies including herceptin [166], dopamine D-4 receptor-targeting antibody [167], bevacizumab [168], and trastuzumab [169]. Kinoshita et al. demonstrated the possibility of delivering various large molecular monoclonal antibodies with penetration through the BBB and into the brain region, including dopamine D-4 receptor-targeting antibody [166] and humanized anti-human epidermal growth factor receptor 2 (HER2/c-erbB2) monoclonal antibody [167]. In addition, it has been reported that enhanced bevacizumab delivery with BBB opening led to a significant increase in animal survival compared to the bevacizumab treatment group alone [168]. Tratuzumab has been IV administered in conjunction with BBB opening in a brain metastasis animal model mimicking HER-2 positive breast cancer. The survival of animals in the ultrasound/tratuzumab group was significantly prolonged compared with the tratuzumab alone group.

Combining MBs with FUS to open the BBB has been successfully translated into clinical evaluations in CNS disease. For the treatment of brain tumor, Carpentier et al. conducted the first clinical trial into BBB opening for enhanced carboplatin delivery in glioblastoma patients using an implant planar ultrasound device (Sonocloud, Catherra) combined with administration of SonoVue (Bracco Imaging SpA). Interim results of a dose-escalating clinical study in a total of 15 patients (NCT02253212) demonstrated successful opening of the BBB at the energy targeted area, sometimes showing hypointense T2*-weighted MRI changes representing occurrence of red blood cell extravasations, and indicated that the

test subjects could tolerate the procedure without adverse events [170]. Idbaih et al. reported a subsequent clinical trial using the same device to enhance carboplatin delivery. A total of 19 patients were recruited and received the BBB opening procedure with a month-based treatment period. Treatment-related adverse events (primarily edema) were reported but were manageable. Patients with successful BBB opening showed progression-free survival of 4.11 months and overall survival of 12.94 months, compared with 2.73 and 8.64 months, respectively, for those without successful BBB opening [171].

Alzheimer's disease treatment

In investigations of MB-ultrasound BBB opening for the treatment of Alzheimer's disease, Raymond et al. first demonstrated BBB opening with the aim of delivering large molecular molecules into an Alzheimer's disease model [172], and Jodao et al. demonstrated BBB opening to enhance delivery of BAM-10 antibodies into the Alzheimer's disease model brain [173]. BBB opening in the hippocampus of animal models of Alzheimer's disease resulted in behavioral improvement that correlated with a reduction of amyloid, combined positive findings of hippocampal neurogenesis [174]. Combining BBB opening with delivery of RN2N tau-specific antibodies as a therapeutic agent resulted in an increase in local concentration of antibody together with a reduction in anxiety-like behavior and phosphorylation [175]. Dubey et al. reported that use of BBB opening to enhance IV Ig delivery resulted in downregulation of the proinflammatory cytokine TNF-α in the hippocampus to modulate the inflammatory effect and boost the neurogenesis effect, in addition to the existing amyloid plaque reduction effect [176]. In a study of opening the BBB alone, Leinenga et al. employed MB-ultrasound to open a wide area of the BBB and observed an apparent plaque burden reduction of up to 75%, with identification of the pathway that activates microglia to speed up clearance of amyloid plaque, and a consequent improvement in memory and behavioral performance [177].

Lipsman et al. and Meng et al. first reported the clinical use of a MR-guided FUS system (Exablate Neuro, Insightec) to open the BBB in the treatment of patients with Alzheimer's disease (NCT02986932 and NCT03671889). Patients with early-to-mild Alzheimer's disease were recruited. Two ultrasound treatments were performed with 1-month intermission and the right dorsolateral prefrontal cortex served as the targeted treatment location. Final follow up was conducted after 3 months. There was no significant difference in beta amyloid burden evaluated by [^{18}F]-florbetaben PET imaging and no clinically significant worsening in cognitive scores at 3 months compared with baseline [178]. Within the same patient group, there was a transient decrease in functional connectivity at the ipsilateral side of the frontoparietal network, but no long-term changes in frontoparietal or default mode network when comparing functional connectivity between the baseline and 3 months [179].

Parkinson's disease treatment

Gene therapy is one potential therapeutic approach for Parkinson's disease. Traditional CNS gene therapy employs the local injection of viral vectors into the CNS target and thus represents an invasive procedure. MB-ultrasound BBB opening shows the capability to deliver large-molecular agents such as mAbs (molecular weight up to 150 kDa) and is a reasonable approach for delivery of therapeutic genomic materials including gene-encoding vectors or RNA interference vectors for genomic-level treatment of diseases such as Parkinson's disease and Huntington's disease.

For RNA interference, Burgess et al. investigated MB-ultrasound BBB opening to enhance the delivery of RNAi and decrease expression of the mutant Huntingtin protein (Htt) [180]. It has been reported that MB-ultrasound BBB opening can successfully be used to deliver reporter genes via viral vectors [181]. Nooroozian et al. demonstrated that MB-ultrasound BBB opening could achieve equivalent gene expression in the brain with a 100-fold reduction in titer compared with intravenous administration of rAAV [182].

Although viral vectors can be successfully used to perform CNS transfection, non-viral vectors such as DNA plasmids conjugated on liposomes provide another option for gene delivery. Lin et al. demonstrated successful expression of reporter gene with the use of gene-loaded liposomes (reporter gene plasmid conjugated with the lipid material to form liposomes) and showed that the expression efficiency could be significantly higher (fivefold) than that achieved via direct injection [183].

Another gene delivery strategy involves the synthesis of lipid-based MBs by conjugating a plasmid together with MBs to form gene-vector MBs or by formation of a liposome MB complex [184, 185]. Of note, a cationic plasmid-MB complex showed improved gene payload and expression of glial cell line-derived neurotrophic factor in the brain via BBB opening, and enhanced therapeutic efficiency when compared with the results using typical microbubbles in a Parkinson's disease animal model. Long et al. employed a different strategy of directly conjugating gene plasmid with the MBs and demonstrated that a therapeutic gene (nuclear factor E2-related factor 2, Nrf2) could be overexpressed in the targeted brain to provide a possible neuroprotective effect in Parkinson's disease model animals [186].

To test the application of MB-ultrasound BBB opening to treat Parkinson's disease dementia, Gasca-Salas et al. conducted a single-arm non-randomized BBB opening clinical trial (NCT03608553) using a MR-guided FUS system

(Exablate Neuro, Insightec; Microbubble: Definity (Bristol-Myers Squibb)). Five patients with Parkinson's disease dementia were recruited with a target region of the right parieto-occipito-temporal cortex, with the designed primary outcome being to assess the safety and success of BBB opening. BBB opening was confirmed with contrast-enhanced MRI, and no adverse effect was reported. Upon examination, mild cognitive improvement was reported although no major changes of the amyloid plaques were detected via [^{18}F]-FDG PET [187, 188].

Neuromodulation and immune modulation

Ultrasound with MBs not only induces BBB opening and permeability changes in endothelial vascular structures and triggers microglia/astrocyte activation, but the mechanical stress from MB cavitation may also enhance neurotransmitter delivery or have a direct post biophysical effect on neurons to induce neural modulation.

McDannold et al. reported that MB-ultrasound BBB opening can enhance the delivery of GABA to temporarily suppress neural activity, and confirmed the neural suppression effect by somatosensory evoked potential [189]. Chu et al. reported that solely inducing MB-ultrasound BBB opening induced a transient neural suppression effect, and confirmed the effect by somatosensory evoked potential and resting-state functional MRI measurement [190]. Similarly, Todd et al. employed resting state blood-oxygen-level-dependent functional MRI to measure functional changes after conducting MB-ultrasound BBB opening and confirmed that regions targeted for BBB opening exhibited local brain functional changes [191]. However, a different observation was reported by Cui et al., who showed that MB-ultrasound interaction resulted in c-fos expression that could excite neuron activity as the c-fos secretion level increased [192]. This observation indicated that neural stimulation originates from the interaction of MB-ultrasound induced amplified radiation force and microstreaming. In a recent clinical trial using MRI-guided FUS to induce BBB opening in patients with Alzheimer's disease, a bilateral change of the frontoparietal networks analyzed by resting state blood-oxygen-level-dependent functional MRI showed a transient decrease in functional connectivity, confirming the neuromodulatory effect of combined use of ultrasound and MBs [179, 193].

To further increase the sensitivity of the neuronal response to ultrasound emission, Ibsen transfected the mechanical sensitive ion channel gene, TRP-4, into *C. elegans* in a strategy termed "sonogenetics". They observed that transfection with TRP-4 increased the responsiveness to MB-ultrasound stimulation, and employed ultrasound stimulation to manipulate the motion trajectory of *C. elegans* [194]. Implementing the sonogenetic concept in mammals, Huang et al. expressed a mechanosensitive gene in a small animal brain [195]. The engineered auditory-sensing protein gene, Prestin, was noninvasively transfected into the brain via MB-ultrasound BBB opening. Once Prestin was expressed in the animal brain an ultrasound mechanical wave could successfully trigger neuron activity, thus demonstrating the feasibility of sonogenetics in vivo.

The mechanical stress induced during MB-ultrasound BBB opening might not only induce an imbalance of vascular circulation-brain extravascular space hemostasis, but also has the potential for triggering an inflammation response. Kovas et al. first demonstrated through transcriptome analysis that this mechanical process triggers expression of the damage-associated molecular pattern response indicating occurrence of a sterile inflammatory response, and further showed that this response stemmed from regulation of the NFκB pathway [196]. McMahon et al. later showed that the effect on transcription was transient and expression had returned to baseline when measured 24 h post-sonication [197]. Of note, it has been reported that the NFκB pathway was only activated in the high MB dose group (100 μL of Definity/kg), indicating that BBB opening with a clinically accepted MB dose (10 μL of Definity/kg) may not induce this inflammatory response [198].

The immunomodulatory effect triggered by MB-ultrasound interaction has been reported to involve the proinflammation pathway. Activation of innate immune cells such as microglia was also reported during the BBB opening process, providing an important mechanism for beta amyloid clearance to benefit Alzheimer's disease treatment. It has also been reported that the anticancer immune response can be modulated to benefit cancer treatment. Focused ultrasound sonication in the presence of MBs has been reported to trigger the recruitment of tumor infiltrating lymphocytes (TILs), including CD4 + CD8 + and CD4 + CD25 + cells, which can be locally detected in higher numbers at the targeted tumors [199]. In addition, Chen also reported that the CD4 + CD8 + cell population as well as the population ratio of CD8/CD25 cells could be significantly increased in glioma tumor models [200, 201].

Phase-change droplets

The use of phase-change droplets with ultrasound also shows potential for theranostic purposes. Phase-change droplets are commonly composed of a lipid shell and a perfluorocarbon liquid core, which has a low boiling point to easily achieve a superheated state for subsequent vaporization [9]. When droplets are subjected to ultrasound stimulation, the pressure variations from the ultrasound wave cause liquid core vaporization and convert droplets into gas bubbles, a process called acoustic droplet vaporization (ADV).

The ADV-generated bubbles (ADV-Bs) present contrast enhancement under ultrasound imaging, suggesting that droplets could be used as an ultrasound contrast agent [202].

Compared with MBs, droplets present a more stable structure and it is easier to make nano-sized particles due to the liquid core [203]. The typical in vivo lifetime of MBs is about 10–20 min, compared with over 90 min for droplets [11]. ADV-Bs are generated through selective ultrasound activation to improve the spatiality and temporality of ultrasound contrast imaging [204]. Since MB-based super-resolution imaging is flow dependent and requires isolated MB distribution (i.e., a low concentration), the acquisition time to sample enough signal in the narrow space of a capillary with low blood flow would be extended [71]. In order to maintain the frame rate of super-resolution imaging, droplets have been utilized as a signal source possessing the required spatial and temporal features upon selective ultrasound activation [205]. The signals of ADV-Bs could accumulate quickly due to the high concentration of droplets and with repeated ultrasound activation, even within vessels without flow [206]. Moreover, the penetration of nano-sized droplets into specific tissue through the leaky vessels might provide localized imaging and treatment of organs or tumors. However, various safety issues including the relatively high energy of ultrasound for ADV [207, 208], the cellular bioeffects of ADV [209, 210], and gas embolisms induced by ADV-Bs [211, 212] might influence the development of droplets for clinical use.

Acoustic droplet vaporization

During the ADV process, nucleation inside the droplet was observed to induce droplet oscillation by high-speed imaging (100–200 ns per frame) [213]. Subsequently, the liquid core of droplets started to vaporize, expand, and finally form bubbles. The expansion ratio of ADV-Bs was approximately 5.0–5.5, and was independent of initial droplet size and ultrasound parameters (acoustic pressures and pulse length) [214]. Similar to the multifunctionality of MBs, the shell of droplets can be modified for specific targeting through changes in surface charge, linkage of antibodies, or conjugation of aptamers. Droplets can encapsulate drugs and locally deliver drugs by triggering ADV [215, 216]. The concurrence of local drug release and ADV-B-enhanced contrast imaging at the target site provides precise theranostic application with real time monitoring during treatment [217].

Correlations between the materials of droplets, droplet size, and acoustic parameters have been investigated to improve the ADV efficiency under low energy ultrasound activation for clinical development. Common materials of the liquid core in droplets include perfluoropropane (C_3F_8), perfluorobutane (C_4F_{10}), perfluoropentane (C_5F_{12}), perfluorohexane (C_6F_{14}), and perfluorooctane (C_8F_{18}) with boiling points of −36.7, −1.7, 29, 56, and 100 °C, respectively [213, 218–221]. Fabiilli et al. fabricated albumin- and lipid-shelled droplets with C_5F_{12}, C_6F_{14}, and C_8F_{16} cores to compare the threshold of ADV [218]. The ADV threshold was directly proportional to the boiling point of the liquid core, inversely proportional to the droplet size, and not affected by the shell materials. To reduce the intensity of ultrasound for ADV, C_4F_{10} and C_3F_8 with lower boiling points have been used to fabricate nanodroplets [222, 223]. Since the boiling points of C_4F_{10} and C_3F_8 are much lower than room temperature, C_4F_{10} and C_3F_8 gas are initially used to make MBs, which are subsequently converted back to nanodroplets by pressurization and condensation. For the same diameter of 300 nm, the ADV threshold was a MI of 2.69 for C_5F_{12} nanodroplets and 1.78 for C_4F_{10} nanodroplets [223]. Moreover, the micro-sized droplets with C_4F_{10} and C_3F_8 core showed ADV with a MI of 0.71 and 0.18, respectively [224]. According to the U.S. Food and Drug Administration guidelines, the maximum intensity for clinical ultrasound diagnosis is a MI of 1.9. The reduced ADV threshold of condensed nanodroplets reveals an opportunity to use a diagnostic ultrasound machine to accomplish ADV in a clinical application.

Cellular bioeffects induced by ADV

The violent mechanical forces produced by the ADV process or ADV-B cavitation can disrupt the cell membrane and cause various bioeffects that assist cellular drug uptake or direct cell death. Wang et al. fabricated aptamer-conjugated and Dox-loaded droplets to target CCRF-CEM human acute lymphoblastic leukemia cells [209]. The droplets were targeted to the cells, where they attached to the cell membrane and induced disruption of cells and release of Dox by ADV to decrease cell viability 4.5-fold. Previous studies investigated the correlation between cell permeability, cell viability, and drug attachment to evaluate the spatial cellular bioeffects induced by ADV. Fan et al. showed a high correlation between the downward pressing region of ADV-Bs and the distribution of dead cells, and between the expansion range of ADV-Bs and the distribution of permeable cells [225]. This demonstrated that the ADV process directly causes cell death by the physical force of ADV-B attachment and enhances membrane permeability of adjacent cells to promote drug uptake. Seda et al. published results consistent with the above study, showing that the size of the ADV-B cloud was directly proportional to the range of cellular damage [210]. These in vitro cellular experiments demonstrate that drug-loaded targeted droplets can combine physical and chemical therapy in a single platform.

Based on these characteristics, a cell-mediated drug delivery system was proposed in which cells uptake droplets and deliver drugs by cell migration. When droplet-loaded

cells migrate into the target regions (i.e., a hypoxic, acidic, or inflammatory tumor microenvironment), intracellular ADV would be triggered by ultrasound to disrupt the carrier cells and distribute the drug locally. The feasibility of droplet uptake into the cytoplasm and intracellular ADV has been proved in macrophages, RAW264.7 cells, and adipose-derived stem cells [226–228]. The ability of cell migration was maintained (32.3–93.3% of controls) after droplet uptake [226, 227, 229]. Disruption of the cell membrane induced by ADV would release the contents of the cytoplasm, including drugs, to promote drug distribution. The in vivo migration ability of droplet-loaded cells was demonstrated in the B16F0 melanoma-bearing mice model [229]. Ultrasound imaging after subcutaneous injection of droplet-loaded cells for 24 h revealed intratumoral contrast enhancement after ADV, providing evidence of cell migration and intracellular ADV in tumors.

Intravascular ADV for gas embolization and antivascular effect

Having considered the in vitro cellular bioeffects induced by ADV, the in vivo bioeffects focusing on vessels are discussed in this section. During the ADV, the mechanical force and expansive ADV-Bs might disrupt the vessel wall or cause gas embolization to induce various physiological effects [230, 231]. Kripfgans et al. detected blood perfusion of rabbit kidney after ADV to evaluate the occurrence of gas embolism [232]. Blood flow in the treated kidney cortex was reduced by 80% at 0 min and recovered to 46% at 90 min. Feng et al. used an ex vivo rat mesentery model to observe intravascular ADV under a confocal acousto-optical high-speed microscope system [212]. Gas embolism and rupture in the vascular lumen were caused by the intravascular ADV-B growth and cavitation, respectively. Rupture and occlusion of vessels blocks oxygen and nutrient delivery, which might induce tissue necrosis and non-reversible side effects after in vivo ADV.

From a different perspective, the vascular bioeffects also provide a potential physical strategy to inhibit tumor growth [11]. Ho et al. used ADV-induced vascular disruption to promote drug penetration into tumors and reported that the intratumoral accumulation of liposomes increased 1.7-fold relative to the control tumors [233]. After disruption of the tumor vasculature, the extravasated droplets could induce intertissue ADV to assist liposome delivery into deep tumor tissue. These results indicate the potential of combining ADV-induced anti-vascular therapy and chemotherapy to produce tumor vessel disruption, immediate drug penetration, and shutdown of blood flow to impede tumor growth. Harmon et al. applied ADV-induced occlusion to inhibit tumor growth in a murine model of hepatocellular carcinoma [211]. After 2 weeks of treatment, histological images of tumor revealed 49.2 ± 7.63, 8.53 ± 4.02, 4.30 ± 3.29, and 0.37 ± 0.37% necrosis in the ADV, ultrasound only, droplet only, and control groups, respectively. The tumor growth rate after ADV was reduced to 37.6% relative to the control tumors, demonstrating the treatment outcome of ADV-induced gas embolotherapy in a tumor model.

Development of nanodroplets for tumor therapy

Since droplets can provide local drug delivery, direct cell disruption, and contrast imaging tracing, tumor therapy is a major application of droplets currently under development. Leaky vessels in the abnormal tumor microenvironment allow nano-sized particles to pass through the gap junction between the endothelial cells and accumulate in tumor tissue, a phenomenon known as the enhanced permeability and retention (EPR) effect [234]. To improve the efficiency of tumor therapy, drug-loaded nanodroplets have been fabricated to increase intratumoral drug accumulation via the EPR effect. In addition, intratumoral ADV might decrease the damage to normal cells around tumors and reduce side effects. Rapoport et al. utilized drug-loaded nanodroplets (300–700 nm) to improve tumor accumulation via the EPR effect, and locally release drug to inhibit tumor growth by the intratumoral ADV [204, 235, 236]. Williams et al. performed IV injection of 220-nm nanodroplets for 1 h accumulation and then observed ADV-B formation within KHT-C sarcoma tumors after ultrasound stimulation (10 MHz, 6 MPa, 1-ms bursts, whole tumor scanning 20 min) [202]. Helfield et al. used C_4F_{10} nanodroplets (diameter 114 ± 1 nm) with MI of 1.7 to observe extravascular ADV within fibrosarcoma via the EPR effect [237]. Since the extravascular nanodroplets could not refill rapidly, the contrast enhancement of intratumoral ADV was activated only once in the short time (30 s). Hence, the absence regions of contrast enhancement on ultrasound imaging after the second ADV presented evidence of nanodroplet extravasation. The intratumoral contrast enhancement on ultrasound imaging induced by the first and second time of ADV was subtracted to quantify the extravascular ADV. The extravasated signal in the fibrosarcoma was 37 ± 5%, which was significantly higher than that in the kidney (-2 ± 8%). Lea-Banks et al. condensed the commercial ultrasound contrast agent Definity (Bristol-Myers Squibb) to fabricate pentobarbital-loaded nanodroplets [238]. The local release of pentobarbital by ADV induced neurosuppression without disrupting the BBB in rats, providing a safety and reproducible method of neuromodulation.

In accordance with the feature of phase-changed droplets, perfluorocarbon with a low boiling point would be vaporized not only by acoustic pressure but also by thermal stimulation. Droplets can also be used as a photothermal agent that can be vaporized through light heating to form

bubbles, produce a mechanical effect, and release drugs, a process called optical droplet vaporization (ODV). Thus, multifunctional PFP nanodroplets have been developed to synergistically combine imaging-guided sono-chemo-photothermal therapy. Hu et al. designed such a strategy using Dox-loaded, polyvinyl alcohol-shelled, and melanin-cored PFP nanodroplets [239]. Melanin is a natural pigment with a known ability to undergo photothermal conversion. When melanin absorbs laser energy, the photothermal effect increases the temperature to assist nanodroplet vaporization under ultrasound stimulation (1.1 MHz, 0.82 MPa). Photoacoustic images of A375 melanoma-bearing mice revealed 2.64-fold higher intratumoral photoacoustic value under opto-acoustic synergistic irradiation relative to the control group, demonstrating bubble formation by ODV/ADV. Histological imaging showed obvious tissue and cell damage in tumors, indicating that the mechanical force induced by ODV/ADV could disrupt tumors. Both photothermal and mechanical effects promoted the release and penetration of Dox to enhance the cytotoxic effect for chemotherapy. The intratumoral accumulation of melanin and Dox in the ODV group was approximately 2.6-fold and 2.0-fold, respectively, relative to the control group.

The feasibility of intratumoral accumulation of nanodroplets and subsequent intratumoral ADV has been demonstrated. To keep the acoustic power as low as possible for development in the clinic, the potential application of MB-condensed nanodroplets has been raised. The in vitro and in vivo results proved the ability of condensed nanodroplet vaporization to provide contrast enhancement on ultrasound imaging. Nevertheless, the stability of condensed nanodroplets should be considered, especially in the application of drug delivery.

Reproducibility of vaporization and recondensation

Although ADV can locally release drugs and enhance cell permeability for drug uptake, the cell damage induced by mechanical force and ADV-B cavitation would be a concerning issue when droplets are applied in the normal tissue or organs. To prevent the induction of non-reversible bioeffects by ADV for in vivo application, MB-condensed nanodroplets were fabricated to control the size of ADV-Bs through regulation of the initial MB generation [240]. Reproducibility of vaporization and recondensation, defined as consecutive vaporization events from a single droplet, was also proposed as a means to repeat the phase change between nanodroplets and MBs and thus avoid the cellular damage induced by the formation of persistent ADV-Bs. The reproducibility of vaporization and recondensation would be influenced by the nanodroplet materials, ultrasound parameters, and temperature [240]. Recondensed nanodroplets with a lower boiling point core (C_4F_{10} and C_3F_8) are easily vaporized to completely form ADV-Bs therefore the investigation of repeated ADV mainly used nanodroplets with a higher boiling point core (C_5F_{12}, C_6F_{14}, and C_8F_{16}). Since the repeated ADV has to precisely control the degree of nucleation inside nanodroplets, the large focus of ultrasound relative to the focus of the laser might be harder to regulate.

Hannah et al. used near-infrared laser to partially heat C_6F_{14} nanodroplets and produce repeated ADV [241]. Optical and ultrasonic imaging showed repeated nanodroplet vaporization and recondensation, which were highly correlated with the irradiation rate of laser pulses. Hallam et al. also used a laser to activate near infrared dye-loaded C_6F_{14} nanodroplets and regulated repeated ADV for BBB opening [242]. The extravasation of Evans blue, photoacoustic imaging, and histological tissue staining in brain indicated the potential of laser-activated repeated ADV as a non-invasive delivery method for brain diagnosis and therapy.

Harmon et al. discussed the retention of phospholipids, PEGlated lipids, and targeting ligands (RGD peptide) on the C_6F_{14} nanodroplet shell during repeated ADV by ultrasound [243]. The size of the nanodroplets was reduced due to shedding of phospholipids but the composition of the targeting ligands and PEGylated lipids was retained after repeated ADV. The retention of targeting ligands and size shrinkage of nanodroplets after repeated ADV might provide enhanced performance in molecular imaging and targeted therapy. Aliabouzar et al. used acoustically responsive scaffolds containing fibrin hydrogels embedded with phase-shift double emulsion microdroplets to investigate the feasibility of payload release by repeated ADV under ultrasound stimulation [244]. Fluorescent dye-loaded C_5F_{12}, C_6F_{14}, and C_8F_{16} nanodroplets were fabricated and the optimal ultrasound parameters for repeated ADV were simulated. The fluorescence intensity of acoustically responsive scaffolds continuously decreased with multiple ultrasound pulses, and the absence of ADV-B formation during ultrasound stimulation indicated the occurrence of repeated ADV. These results demonstrated that C_6F_{14} and C_8F_{16} nanodroplets could continuously release payload during repeated ADV.

Conclusion and future development

Medical ultrasound imaging is a mature diagnostic imaging modality in current clinical use. New clinical applications of ultrasound imaging such as high-resolution elastography, functional blood flow imaging, and molecular imaging are constantly being developed to provide physiological information. Among drug carriers, MBs and droplets with several special properties can easily be integrated with medical ultrasound to achieve noninvasive imaging and therapy at the same time. In particular, therapeutic ultrasound combined with MBs provides a new

opportunity to realize noninvasive opening of the CNS barrier for therapeutic agent delivery. This concept has been under development for almost two decades and is now under clinical evaluation. In addition, preclinical evidence supports other possible applications, including anticancer immune modulation and neuromodulation. The future clinical applications of MBs can be further expanded by: (1) designing a transducer with trapping, therapeutic, and imaging abilities; and (2) improving the physical stability and payload capacity of MBs. Moreover, the applications of phase-change droplets in tumor and CNS therapy have evolved and matured. The balance between local drug delivery and biosafety has been improved by modifying the initial micro-sized droplets to nano-sized, condensed, and repeated-ADV droplets. Although the use of MBs with ultrasound for theranostic purposes seems to have developed faster and has already entered clinical evaluation, it is recognized that the use of droplets in conjunction with ultrasound presents numerous strengths such as sustained drug release, enhanced cell permeability, and improved ultrasound imaging without sacrificing safety. It is highly anticipated that the combined use of ADV and ultrasound will have clinical value in the near future.

Acknowledgements The authors gratefully acknowledge the support of the Ministry of Science and Technology, Taiwan under Grant No. MOST 108-2221-E-007-040-MY3, 108-2221-E-007-041-MY3, 108-2638-M-002-001-MY2, 107-2628-E-006-004-MY3, 107-2221-E-006-024-MY3, 109-2636-E-006-024-, 110-2321-B-002-010-, 108-2221-E-002-176-MY3, and 108-2221-E-002-175-MY3; National Tsing Hua University under Grant No. 110Q2510E1. The authors also thank to support from Higher Education Sprout Project, Ministry of Education to the Headquarters of University Advancement at NCKU.

Author contributions Y.J. H and C.K. Y conceptualised the manuscript, Y.J. H, C.C. H, C.H. F, and H. L. L wrote the manuscript, C.C. H, C.H. F and H. L. L designed and prepared the tables and figures. All authors reviewed and edited the final version of the text and approved the final manuscript.

Funding This work was supported by the Ministry of Science and Technology, Taiwan (Grant No. MOST 108-2221-E-007-040-MY3, 108-2221-E-007-041-MY3, 108-2638-M-002-001-MY2, 107-2628-E-006-004-MY3, 107-2221-E-006-024-MY3, 109-2636-E-006-024-, 110-2321-B-002-010-, 108-2221-E-002-176-MY3, and 108-2221-E-002-175-MY3), National Tsing Hua University (Grant No. 110Q2510E1), and Headquarters of University Advancement at NCKU.

Availability of data and material Not applicable.

Code availability Not applicable.

Declarations

Conflict of interest The authors declare that they have no conflict of interest.

Ethical approval Not applicable.

Consent to participate Not applicable.

Consent for publication Not applicable.

References

1. Leighton TG (2007) What is ultrasound? Prog Biophys Mol Biol 93:3–83. https://doi.org/10.1016/j.pbiomolbio.2006.07.026
2. Shung KK (2006) Diagnostic Ultrasound: Imaging and blood flow measurement. CRC Press, Boca Raton
3. Ignee A, Atkinson NS, Schuessler G, Dietrich CF (2016) Ultrasound contrast agents. Endosc Ultrasound 5:355–362. https://doi.org/10.4103/2303-9027.193594
4. Bercoff J (2011) Ultrafast ultrasound imaging. IntechOpen
5. Lentacker I, De Cock I, Deckers R, De Smedt SC, Moonen CT (2014) Understanding ultrasound induced sonoporation: definitions and underlying mechanisms. Adv Drug Deliv Rev 72:49–64. https://doi.org/10.1016/j.addr.2013.11.008
6. Deprez J, Lajoinie G, Engelen Y, De Smedt SC, Lentacker I (2021) Opening doors with ultrasound and microbubbles: Beating biological barriers to promote drug delivery. Adv Drug Deliv Rev 172:9–36. https://doi.org/10.1016/j.addr.2021.02.015
7. Liu HL, Fan CH, Ting CY, Yeh CK (2014) Combining microbubbles and ultrasound for drug delivery to brain tumors: current progress and overview. Theranostics 4:432–444. https://doi.org/10.7150/thno.8074
8. Meng Y, Hynynen K, Lipsman N (2021) Applications of focused ultrasound in the brain: from thermoablation to drug delivery. Nat Rev Neurol 17:7–22. https://doi.org/10.1038/s41582-020-00418-z
9. Kripfgans OD, Fowlkes JB, Miller DL, Eldevik OP, Carson PL (2000) Acoustic droplet vaporization for therapeutic and diagnostic applications. Ultrasound Med Biol 26:1177–1189
10. Huynh E, Rajora MA, Zheng G (2016) Multimodal micro, nano, and size conversion ultrasound agents for imaging and therapy. Wiley Interdiscip Rev Nanomed Nanobiotechnol 8:796–813. https://doi.org/10.1002/wnan.1398
11. Ho YJ, Wang TC, Fan CH, Yeh CK (2017) Current progress in antivascular tumor therapy. Drug Discov Today 22:1503–1515. https://doi.org/10.1016/j.drudis.2017.06.001
12. Lea-Banks H, O'Reilly MA, Hynynen K (2019) Ultrasound-responsive droplets for therapy: A review. J Control Release 293:144–154. https://doi.org/10.1016/j.jconrel.2018.11.028
13. Wells PNT (1977) Biomedical ultrasonics. Academic Press, London
14. Shung KK, Smith M, Tsui BMW (1992) Principles of Medical Imaging. Academic Press, San Diego
15. Shung KK, Thieme GA (1993) Biological tissues as ultrasonic scattering media. CRC Press, Boca Raton
16. Hill JC, Palma RA (2005) Doppler tissue imaging for the assessment of left ventricular diastolic function: a systematic approach for the sonographer. J Am Soc Echocardiogr 18:80–88. https://doi.org/10.1016/j.echo.2004.09.007
17. Ommen SR, Nishimura RA, Appleton CP, Miller FA, Oh JK, Redfield MM et al (2000) Clinical utility of Doppler echocardiography and tissue Doppler imaging in the estimation of left ventricular filling pressures: A comparative simultaneous Doppler-catheterization study. Circulation 102:1788–1794. https://doi.org/10.1161/01.cir.102.15.1788
18. Sohn DW, Chai IH, Lee DJ, Kim HC, Kim HS, Oh BH et al (1997) Assessment of mitral annulus velocity by Doppler tissue

imaging in the evaluation of left ventricular diastolic function. J Am Coll Cardiol 30:474–480. https://doi.org/10.1016/s0735-1097(97)88335-0
19. Greenleaf JA (1986) Tissue characterization with ultrasound. CRC Press, Boca Raton
20. Tanter M, Fink M (2014) Ultrafast imaging in biomedical ultrasound. IEEE Trans Ultrason Ferroelectr Freq Control 61:102–119. https://doi.org/10.1109/TUFFC.2014.6689779
21. Fink M (1983) Ultrasound imaging. Revue De Physique Appliquee 18:527–556. https://doi.org/10.1051/rphysap:01983001809052700
22. Lu JY, Greenleaf JF (1991) Pulse-echo imaging using a nondiffracting beam transducer. Ultrasound Med Biol 17:265–281. https://doi.org/10.1016/0301-5629(91)90048-2
23. Tanter M, Bercoff J, Sandrin L, Fink M (2002) Ultrafast compound imaging for 2-D motion vector estimation: application to transient elastography. IEEE Trans Ultrason Ferroelectr Freq Control 49:1363–1374. https://doi.org/10.1109/tuffc.2002.1041078
24. Huang CC, Chen PY, Peng PH, Lee PY (2017) 40 MHz high-frequency ultrafast ultrasound imaging. Med Phys 44:2185–2195. https://doi.org/10.1002/mp.12244
25. Ophir J, Alam SK, Garra B, Kallel F, Konofagou E, Krouskop T et al (1999) Elastography: ultrasonic estimation and imaging of the elastic properties of tissues. Proc Inst Mech Eng H 213:203–233. https://doi.org/10.1243/0954411991534933
26. Nightingale K, Soo MS, Nightingale R, Trahey G (2002) Acoustic radiation force impulse imaging: in vivo demonstration of clinical feasibility. Ultrasound Med Biol 28:227–235. https://doi.org/10.1016/s0301-5629(01)00499-9
27. Gao L, Parker KJ, Lerner RM, Levinson SF (1996) Imaging of the elastic properties of tissue–a review. Ultrasound Med Biol 22:959–977. https://doi.org/10.1016/s0301-5629(96)00120-2
28. Nightingale KR, Palmeri ML, Nightingale RW, Trahey GE (2001) On the feasibility of remote palpation using acoustic radiation force. J Acoust Soc Am 110:625–634. https://doi.org/10.1121/1.1378344
29. Nightingale KR, Kornguth PJ, Trahey GE (1999) The use of acoustic streaming in breast lesion diagnosis: A clinical study. Ultrasound Med Biol 25:75–87. https://doi.org/10.1016/S0301-5629(98)00152-5
30. Walker WF (1999) Internal deformation of a uniform elastic solid by acoustic radiation force. J Acoust Soc Am 105:2508–2518. https://doi.org/10.1121/1.426854
31. Fatemi M, Greenleaf JF (1999) Vibro-acoustography: an imaging modality based on ultrasound-stimulated acoustic emission. Proc Natl Acad Sci U S A 96:6603–6608. https://doi.org/10.1073/pnas.96.12.6603
32. Huang CC, Shih CC, Liu TY, Lee PY (2011) Assessing the viscoelastic properties of thrombus using a solid-sphere-based instantaneous force approach. Ultrasound Med Biol 37:1722–1733. https://doi.org/10.1016/j.ultrasmedbio.2011.06.026
33. Fahey BJ, Nightingale KR, Stutz DL, Trahey GE (2004) Acoustic radiation force impulse imaging of thermally- and chemically-induced lesions in soft tissues: preliminary ex vivo results. Ultrasound Med Biol 30:321–328. https://doi.org/10.1016/j.ultrasmedbio.2003.11.012
34. Shih CC, Huang CC, Zhou Q, Shung KK (2013) High-resolution acoustic-radiation-force-impulse imaging for assessing corneal sclerosis. IEEE Trans Med Imag 32:1316–1324. https://doi.org/10.1109/TMI.2013.2256794
35. Gennisson JL, Deffieux T, Mace E, Montaldo G, Fink M, Tanter M (2010) Viscoelastic and anisotropic mechanical properties of in vivo muscle tissue assessed by supersonic shear imaging. Ultrasound Med Biol 36:789–801. https://doi.org/10.1016/j.ultrasmedbio.2010.02.013
36. Muller M, Gennisson JL, Deffieux T, Tanter M, Fink M (2009) Quantitative viscoelasticity mapping of human liver using supersonic shear imaging: preliminary in vivo feasibility study. Ultrasound Med Biol 35:219–229. https://doi.org/10.1016/j.ultrasmedbio.2008.08.018
37. Tanter M, Bercoff J, Athanasiou A, Deffieux T, Gennisson JL, Montaldo G et al (2008) Quantitative assessment of breast lesion viscoelasticity: initial clinical results using supersonic shear imaging. Ultrasound Med Biol 34:1373–1386. https://doi.org/10.1016/j.ultrasmedbio.2008.02.002
38. Nomikou N, Tiwari P, Trehan T, Gulati K, McHale AP (2012) Studies on neutral, cationic and biotinylated cationic microbubbles in enhancing ultrasound-mediated gene delivery in vitro and in vivo. Acta Biomater 8:1273–1280. https://doi.org/10.1016/j.actbio.2011.09.010
39. Cebi Olgun D, Korkmazer B, Kilic F, Dikici AS, Velidedeoglu M, Aydogan F et al (2014) Use of shear wave elastography to differentiate benign and malignant breast lesions. Diagn Interv Radiol 20:239–244. https://doi.org/10.5152/dir.2014.13306
40. Balleyguier C, Ciolovan L, Ammari S, Canale S, Sethom S, Al Rouhbane R et al (2013) Breast elastography: the technical process and its applications. Diagn Interv Imag 94:503–513. https://doi.org/10.1016/j.diii.2013.02.006
41. Samir AE, Dhyani M, Vij A, Bhan AK, Halpern EF, Mendez-Navarro J et al (2015) Shear-wave elastography for the estimation of liver fibrosis in chronic liver disease: determining accuracy and ideal site for measurement. Radiology 274:888–896. https://doi.org/10.1148/radiol.14140839
42. Sande JA, Verjee S, Vinayak S, Amersi F, Ghesani M (2017) Ultrasound shear wave elastography and liver fibrosis: A Prospective Multicenter Study. World J Hepatol 9:38–47. https://doi.org/10.4254/wjh.v9.i1.38
43. Park AY, Son EJ, Han K, Youk JH, Kim JA, Park CS (2015) Shear wave elastography of thyroid nodules for the prediction of malignancy in a large scale study. Eur J Radiol 84:407–412. https://doi.org/10.1016/j.ejrad.2014.11.019
44. Chen PY, Yang TH, Kuo LC, Shih CC, Huang CC (2020) Characterization of hand tendons through high-frequency ultrasound elastography. IEEE Trans Ultrason Ferroelectr Freq Control 67:37–48. https://doi.org/10.1109/Tuffc.2019.2938147
45. Chen PY, Shih CC, Lin WC, Ma T, Zhou QF, Shung KK et al (2018) High-resolution shear wave imaging of the human cornea using a dual-element transducer. Sensors. https://doi.org/10.3390/s18124244
46. Shih CC, Qian XJ, Ma T, Han ZL, Huang CC, Zhou QF et al (2018) Quantitative assessment of thin-layer tissue viscoelastic properties using ultrasonic micro-elastography with lamb wave model. IEEE Trans Med Imag 37:1887–1898. https://doi.org/10.1109/Tmi.2018.2820157
47. Tanter M, Touboul D, Gennisson JL, Bercoff J, Fink M (2009) High-resolution quantitative imaging of cornea elasticity using supersonic shear imaging. IEEE Trans Med Imag 28:1881–1893. https://doi.org/10.1109/TMI.2009.2021471
48. Huang CC, Chen PY, Shih CC (2013) Estimating the viscoelastic modulus of a thrombus using an ultrasonic shear-wave approach. Med Phys 40:042901. https://doi.org/10.1118/1.4794493
49. Shih CC, Chen PY, Ma T, Zhou Q, Shung KK, Huang CC (2018) Development of an intravascular ultrasound elastography based on a dual-element transducer. R Soc Open Sci 5:180138. https://doi.org/10.1098/rsos.180138
50. Sun L, Lien CL, Xu X, Shung KK (2008) In vivo cardiac imaging of adult zebrafish using high frequency ultrasound (45–75 MHz). Ultrasound Med Biol 34:31–39. https://doi.org/10.1016/j.ultrasmedbio.2007.07.002
51. Liu TY, Lee PY, Huang CC, Sun L, Shung KK (2013) A study of the adult zebrafish ventricular function by retrospective

Doppler-gated ultrahigh-frame-rate echocardiography. IEEE Trans Ultrason Ferroelectr Freq Control 60:1827–1837. https://doi.org/10.1109/TUFFC.2013.2769
52. Sun P, Zhang Y, Yu F, Parks E, Lyman A, Wu Q et al (2009) Micro-electrocardiograms to study post-ventricular amputation of zebrafish heart. Ann Biomed Eng 37:890–901. https://doi.org/10.1007/s10439-009-9668-3
53. Huang CC, Su TH, Shih CC (2015) High-resolution tissue Doppler imaging of the zebrafish heart during its regeneration. Zebrafish 12:48–57. https://doi.org/10.1089/zeb.2014.1026
54. Ho-Chiang C, Huang H, Huang CC (2020) High-frequency ultrasound deformation imaging for adult zebrafish during heart regeneration. Quant Imaging Med Surg 10: 66–75. https://doi.org/10.21037/qims.2019.09.20
55. Fei CL, Chiu CT, Chen XY, Chen ZY, Ma JG, Zhu BP et al (2016) Ultrahigh Frequency (100 MHz-300 MHz) Ultrasonic Transducers for Optical Resolution Medical Imagining. Sci Rep 6 ARTN 28360 https://doi.org/10.1038/srep28360
56. Mohamed ETA, Declercq NF (2020) Giga-Hertz ultrasonic microscopy: Getting over the obscurity- A short review on the biomedical applications. Phys Med 9:100025. https://doi.org/10.1016/j.phmed.2020.100025
57. Ingram N, Macnab SA, Marston G, Scott N, Carr IM, Markham AF et al (2013) The use of high-frequency ultrasound imaging and biofluorescence for in vivo evaluation of gene therapy vectors. BMC Med Imag 13:35. https://doi.org/10.1186/1471-2342-13-35
58. Lakshman M, Needles A (2015) Screening and quantification of the tumor microenvironment with micro-ultrasound and photoacoustic imaging. Nat Methods 12:iii–v
59. Huang CC, Cheng HF, Zhu BP, Chen PY, Beh ST, Kuo YM et al (2017) Studying arterial stiffness using high-frequency ultrasound in mice with alzheimer disease. Ultrasound Med Biol 43:2054–2064. https://doi.org/10.1016/j.ultrasmedbio.2017.04.029
60. Huang CC, Chen WT (2014) Developing high-frequency ultrasound tomography for testicular tumor imaging in rats: an in vitro study. Med Phys 41:012902. https://doi.org/10.1118/1.4852915
61. Chang CC, Chen PY, Huang H, Huang CC (2019) In Vivo Visualization of vasculature in adult zebrafish by using high-frequency ultrafast ultrasound imaging. IEEE Trans Biomed Eng 66:1742–1751. https://doi.org/10.1109/Tbme.2018.2878887
62. Hsiao YY, Yang TH, Chen PY, Hsu HY, Kuo LC, Su FC et al (2020) Characterization of the extensor digitorum communis tendon using high-frequency ultrasound shear wave elastography. Med Phys. https://doi.org/10.1002/mp.14061
63. Huang H, Chen PY, Huang CC (2020) 40-MHz high-frequency vector Doppler imaging for superficial venous valve flow estimation. Med Phys 47:4020–4031. https://doi.org/10.1002/mp.14362
64. Lay FY, Chen PY, Cheng HF, Kuo YM, Huang CC (2019) Ex vivo evaluation of mouse brain elasticity using high-frequency ultrasound elastography. IEEE Trans Biomed Eng 66:3426–3435. https://doi.org/10.1109/Tbme.2019.2905551
65. Li HC, Chen PY, Cheng HF, Kuo YM, Huang CC (2019) In Vivo visualization of brain vasculature in alzheimer's disease mice by high-frequency micro-doppler imaging. IEEE Trans Biomed Eng 66:3393–3401. https://doi.org/10.1109/Tbme.2019.2904702
66. Wang MY, Yang TH, Huang H, Hsu HY, Kuo LC, Su FC et al (2020) Evaluation of hand tendon movement by using high-frequency ultrasound vector doppler imaging. IEEE Trans Biomed Eng 67:2945–2952. https://doi.org/10.1109/Tbme.2020.2974244
67. Frinking P, Segers T, Luan Y, Tranquart F (2020) Three decades of ultrasound contrast agents: a review of the past, present and future improvements. Ultrasound Med Biol 46:892–908. https://doi.org/10.1016/j.ultrasmedbio.2019.12.008
68. Nguyen T, Davidson BP (2019) Contrast enhanced ultrasound perfusion imaging in skeletal muscle. J Cardiovasc Imaging 27:163–177. https://doi.org/10.4250/jcvi.2019.27.e31
69. Rafailidis V, Huang DY, Yusuf GT, Sidhu PS (2020) General principles and overview of vascular contrast-enhanced ultrasonography. Ultrasonography 39: 22–42. https://doi.org/10.14366/usg.19022
70. Schinkel AFL, Bosch JG, Staub D, Adam D, Feinstein SB (2020) Contrast-enhanced ultrasound to assess carotid intraplaque neovascularization. Ultrasound Med Biol 46:466–478. https://doi.org/10.1016/j.ultrasmedbio.2019.10.020
71. Christensen-Jeffries K, Couture O, Dayton PA, Eldar YC, Hynynen K, Kiessling F et al (2020) Super-resolution Ultrasound Imaging. Ultrasound Med Biol 46:865–891. https://doi.org/10.1016/j.ultrasmedbio.2019.11.013
72. Dizeux A, Gesnik M, Ahnine H, Blaize K, Arcizet F, Picaud S et al (2019) Functional ultrasound imaging of the brain reveals propagation of task-related brain activity in behaving primates. Nat Commun 10:1400. https://doi.org/10.1038/s41467-019-09349-w
73. Errico C, Pierre J, Pezet S, Desailly Y, Lenkei Z, Couture O et al (2015) Ultrafast ultrasound localization microscopy for deep super-resolution vascular imaging. Nature 527:499–502. https://doi.org/10.1038/nature16066
74. Couture O, Hingot V, Heiles B, Muleki-Seya P, Tanter M (2018) Ultrasound localization microscopy and super-resolution: a state of the art. IEEE Trans Ultrason Ferroelectr Freq Control 65:1304–1320. https://doi.org/10.1109/TUFFC.2018.2850811
75. Lin CY, Tsai CH, Feng LY, Chai WY, Lin CJ, Huang CY et al (2019) Focused ultrasound-induced blood brain-barrier opening enhanced vascular permeability for GDNF delivery in Huntington's disease mouse model. Brain Stimul 12:1143–1150. https://doi.org/10.1016/j.brs.2019.04.011
76. Geers B, Lentacker I, Sanders NN, Demeester J, Meairs S, De Smedt SC (2011) Self-assembled liposome-loaded microbubbles: The missing link for safe and efficient ultrasound triggered drug-delivery. J Control Release 152:249–256. https://doi.org/10.1016/j.jconrel.2011.02.024
77. Ting CY, Fan CH, Liu HL, Huang CY, Hsieh HY, Yen TC et al (2012) Concurrent blood-brain barrier opening and local drug delivery using drug-carrying microbubbles and focused ultrasound for brain glioma treatment. Biomaterials 33:704–712. https://doi.org/10.1016/j.biomaterials.2011.09.096
78. Unger EC, McCreery TP, Sweitzer RH, Caldwell VE, Wu Y (1998) Acoustically active lipospheres containing paclitaxel: a new therapeutic ultrasound contrast agent. Invest Radiol 33:886–892. https://doi.org/10.1097/00004424-199812000-00007
79. Fan CH, Ting CY, Liu HL, Huang CY, Hsieh HY, Yen TC et al (2013) Antiangiogenic-targeting drug-loaded microbubbles combined with focused ultrasound for glioma treatment. Biomaterials 34:2142–2155. https://doi.org/10.1016/j.biomaterials.2012.11.048
80. Yeh JS, Sennoga CA, McConnell E, Eckersley R, Tang MX, Nourshargh S et al (2015) A targeting microbubble for ultrasound molecular imaging. PLoS ONE 10:e0129681. https://doi.org/10.1371/journal.pone.0129681
81. Tinkov S, Coester C, Serba S, Geis NA, Katus HA, Winter G et al (2010) New doxorubicin-loaded phospholipid microbubbles for targeted tumor therapy: in-vivo characterization. J Control Release 148:368–372. https://doi.org/10.1016/j.jconrel.2010.09.004
82. Shortencarier MJ, Dayton PA, Bloch SH, Schumann PA, Matsunaga TO, Ferrara KW (2004) A method for radiation-force localized drug delivery using gas-filled lipospheres. IEEE Trans Ultrason Ferroelectr Freq Control 51:822–831. https://doi.org/10.1109/tuffc.2004.1320741

83. Borden MA, Caskey CF, Little E, Gillies RJ, Ferrara KW (2007) DNA and polylysine adsorption and multilayer construction onto cationic lipid-coated microbubbles. Langmuir 23:9401–9408. https://doi.org/10.1021/la7009034
84. Melino S, Zhou M, Tortora M, Paci M, Cavalieri F, Ashokkumar M (2012) Molecular properties of lysozyme-microbubbles: towards the protein and nucleic acid delivery. Amino Acids 43:885–896. https://doi.org/10.1007/s00726-011-1148-z
85. Liao AH, Hung CR, Lin CF, Lin YC, Chen HK (2017) Treatment effects of lysozyme-shelled microbubbles and ultrasound in inflammatory skin disease. Sci Rep 7:41325. https://doi.org/10.1038/srep41325
86. Lum AF, Borden MA, Dayton PA, Kruse DE, Simon SI, Ferrara KW (2006) Ultrasound radiation force enables targeted deposition of model drug carriers loaded on microbubbles. J Control Release 111:128–134. https://doi.org/10.1016/j.jconrel.2005.11.006
87. Ryu JY, Won EJ, Lee HAR, Kim JH, Hui E, Kim HP et al (2020) Ultrasound-activated particles as CRISPR/Cas9 delivery system for androgenic alopecia therapy. Biomaterials 232:119736. https://doi.org/10.1016/j.biomaterials.2019.119736
88. Ho YJ, Chu SW, Liao EC, Fan CH, Chan HL, Wei KC et al (2019) Normalization of tumor vasculature by oxygen microbubbles with ultrasound. Theranostics 9:7370–7383. https://doi.org/10.7150/thno.37750
89. Ho YJ, Wang TC, Fan CH, Yeh CK (2018) Spatially uniform tumor treatment and drug penetration by regulating ultrasound with microbubbles. ACS Appl Mater Interfaces 10:17784–17791. https://doi.org/10.1021/acsami.8b05508
90. McEwan C, Owen J, Stride E, Fowley C, Nesbitt H, Cochrane D et al (2015) Oxygen carrying microbubbles for enhanced sonodynamic therapy of hypoxic tumours. J Control Release 203:51–56. https://doi.org/10.1016/j.jconrel.2015.02.004
91. Grishenkov D, Gonon A, Weitzberg E, Lundberg JO, Harmark J, Cerroni B et al (2015) Ultrasound contrast agent loaded with nitric oxide as a theranostic microdevice. Drug Des Devel Ther 9:2409–2419. https://doi.org/10.2147/DDDT.S77790
92. Huynh E, Leung BY, Helfield BL, Shakiba M, Gandier JA, Jin CS et al (2015) In situ conversion of porphyrin microbubbles to nanoparticles for multimodality imaging. Nat Nanotechnol 10:325–332. https://doi.org/10.1038/nnano.2015.25
93. Fan CH, Chang EL, Ting CY, Lin YC, Liao EC, Huang CY et al (2016) Folate-conjugated gene-carrying microbubbles with focused ultrasound for concurrent blood-brain barrier opening and local gene delivery. Biomaterials 106:46–57. https://doi.org/10.1016/j.biomaterials.2016.08.017
94. Luan Y, Lajoinie G, Gelderblom E, Skachkov I, van der Steen AF, Vos HJ et al (2014) Lipid shedding from single oscillating microbubbles. Ultrasound Med Biol 40:1834–1846. https://doi.org/10.1016/j.ultrasmedbio.2014.02.031
95. De Cock I, Lajoinie G, Versluis M, De Smedt SC, Lentacker I (2016) Sonoprinting and the importance of microbubble loading for the ultrasound mediated cellular delivery of nanoparticles. Biomaterials 83:294–307. https://doi.org/10.1016/j.biomaterials.2016.01.022
96. Roovers S, Lajoinie G, De Cock I, Brans T, Dewitte H, Braeckmans K et al (2019) Sonoprinting of nanoparticle-loaded microbubbles: Unraveling the multi-timescale mechanism. Biomaterials 217:119250. https://doi.org/10.1016/j.biomaterials.2019.119250
97. Roovers S, Deprez J, Priwitaningrum D, Lajoinie G, Rivron N, Declercq H et al (2019) Sonoprinting liposomes on tumor spheroids by microbubbles and ultrasound. J Control Release 316:79–92. https://doi.org/10.1016/j.jconrel.2019.10.051
98. De Temmerman ML, Dewitte H, Vandenbroucke RE, Lucas B, Libert C, Demeester J et al (2011) mRNA-Lipoplex loaded microbubble contrast agents for ultrasound-assisted transfection of dendritic cells. Biomaterials 32:9128–9135. https://doi.org/10.1016/j.biomaterials.2011.08.024
99. Helfield B, Chen X, Watkins SC, Villanueva FS (2016) Biophysical insight into mechanisms of sonoporation. Proc Natl Acad Sci U S A 113:9983–9988. https://doi.org/10.1073/pnas.1606915113
100. Apodaca G (2002) Modulation of membrane traffic by mechanical stimuli. Am J Physiol Renal Physiol 282:F179-190. https://doi.org/10.1152/ajprenal.2002.282.2.F179
101. Sutton JT, Haworth KJ, Pyne-Geithman G, Holland CK (2013) Ultrasound-mediated drug delivery for cardiovascular disease. Expert Opin Drug Deliv 10:573–592. https://doi.org/10.1517/17425247.2013.772578
102. Kooiman K, Vos HJ, Versluis M, de Jong N (2014) Acoustic behavior of microbubbles and implications for drug delivery. Adv Drug Deliv Rev 72:28–48. https://doi.org/10.1016/j.addr.2014.03.003
103. Qin P, Han T, Yu ACH, Xu L (2018) Mechanistic understanding the bioeffects of ultrasound-driven microbubbles to enhance macromolecule delivery. J Control Release 272:169–181. https://doi.org/10.1016/j.jconrel.2018.01.001
104. Qin S, Caskey CF, Ferrara KW (2009) Ultrasound contrast microbubbles in imaging and therapy: physical principles and engineering. Phys Med Biol 54:R27-57. https://doi.org/10.1088/0031-9155/54/6/R01
105. Zhao YZ, Luo YK, Lu CT, Xu JF, Tang J, Zhang M et al (2008) Phospholipids-based microbubbles sonoporation pore size and reseal of cell membrane cultured in vitro. J Drug Target 16:18–25. https://doi.org/10.1080/10611860701637792
106. Deng CX, Sieling F, Pan H, Cui J (2004) Ultrasound-induced cell membrane porosity. Ultrasound Med Biol 30:519–526. https://doi.org/10.1016/j.ultrasmedbio.2004.01.005
107. Hu Y, Wan JM, Yu AC (2013) Membrane perforation and recovery dynamics in microbubble-mediated sonoporation. Ultrasound Med Biol 39:2393–2405. https://doi.org/10.1016/j.ultrasmedbio.2013.08.003
108. Lionetti V, Fittipaldi A, Agostini S, Giacca M, Recchia FA, Picano E (2009) Enhanced caveolae-mediated endocytosis by diagnostic ultrasound in vitro. Ultrasound Med Biol 35:136–143. https://doi.org/10.1016/j.ultrasmedbio.2008.07.011
109. Zeghimi A, Escoffre JM, Bouakaz A (2015) Role of endocytosis in sonoporation-mediated membrane permeabilization and uptake of small molecules: a electron microscopy study. Phys Biol 12:066007. https://doi.org/10.1088/1478-3975/12/6/066007
110. Fekri F, Delos Santos RC, Karshafian R, Antonescu CN (2016) Ultrasound microbubble treatment enhances clathrin-mediated endocytosis and fluid-phase uptake through distinct mechanisms. PLoS ONE 11:e0156754. https://doi.org/10.1371/journal.pone.0156754
111. Davies PF, Dewey CF Jr, Bussolari SR, Gordon EJ, Gimbrone MA Jr (1984) Influence of hemodynamic forces on vascular endothelial function. In vitro studies of shear stress and pinocytosis in bovine aortic cells. J Clin Invest 73:1121–1129. https://doi.org/10.1172/JCI111298
112. Ho YJ, Chang HC, Lin CW, Fan CH, Lin YC, Wei KC et al (2021) Oscillatory behavior of microbubbles impacts efficacy of cellular drug delivery. J Control Release 333:316–327. https://doi.org/10.1016/j.jconrel.2021.03.044
113. Davies PF (1995) Flow-mediated endothelial mechanotransduction. Physiol Rev 75:519–560. https://doi.org/10.1152/physrev.1995.75.3.519
114. Wu J (2002) Theoretical study on shear stress generated by microstreaming surrounding contrast agents attached to living cells. Ultrasound Med Biol 28:125–129. https://doi.org/10.1016/s0301-5629(01)00497-5

115. Caskey CF, Qin S, Dayton PA, Ferrara KW (2009) Microbubble tunneling in gel phantoms. J Acoust Soc Am 125:183–189. https://doi.org/10.1121/1.3097679
116. Arvanitis CD, Bazan-Peregrino M, Rifai B, Seymour LW, Coussios CC (2011) Cavitation-enhanced extravasation for drug delivery. Ultrasound Med Biol 37:1838–1852. https://doi.org/10.1016/j.ultrasmedbio.2011.08.004
117. Heath CH, Sorace A, Knowles J, Rosenthal E, Hoyt K (2012) Microbubble therapy enhances anti-tumor properties of cisplatin and cetuximab in vitro and in vivo. Otolaryngol Head Neck Surg 146:938–945. https://doi.org/10.1177/0194599812436648
118. Sakakima Y, Hayashi S, Yagi Y, Hayakawa A, Tachibana K, Nakao A (2005) Gene therapy for hepatocellular carcinoma using sonoporation enhanced by contrast agents. Cancer Gene Ther 12:884–889. https://doi.org/10.1038/sj.cgt.7700850
119. Zolochevska O, Xia X, Williams BJ, Ramsay A, Li S, Figueiredo ML (2011) Sonoporation delivery of interleukin-27 gene therapy efficiently reduces prostate tumor cell growth in vivo. Hum Gene Ther 22:1537–1550. https://doi.org/10.1089/hum.2011.076
120. Suzuki R, Namai E, Oda Y, Nishiie N, Otake S, Koshima R et al (2010) Cancer gene therapy by IL-12 gene delivery using liposomal bubbles and tumoral ultrasound exposure. J Control Release 142:245–250. https://doi.org/10.1016/j.jconrel.2009.10.027
121. Suzuki R, Oda Y, Utoguchi N, Namai E, Taira Y, Okada N et al (2009) A novel strategy utilizing ultrasound for antigen delivery in dendritic cell-based cancer immunotherapy. J Control Release 133:198–205. https://doi.org/10.1016/j.jconrel.2008.10.015
122. Oda Y, Suzuki R, Otake S, Nishiie N, Hirata K, Koshima R et al (2012) Prophylactic immunization with Bubble liposomes and ultrasound-treated dendritic cells provided a four-fold decrease in the frequency of melanoma lung metastasis. J Control Release 160:362–366. https://doi.org/10.1016/j.jconrel.2011.12.003
123. Kotopoulis S, Delalande A, Popa M, Mamaeva V, Dimcevski G, Gilja OH et al (2014) Sonoporation-enhanced chemotherapy significantly reduces primary tumour burden in an orthotopic pancreatic cancer xenograft. Mol Imag Biol 16:53–62. https://doi.org/10.1007/s11307-013-0672-5
124. Couture O, Foley J, Kassell NF, Larrat B, Aubry JF (2014) Review of ultrasound mediated drug delivery for cancer treatment: updates from pre-clinical studies. Trans Cancer Res 3:494–511. https://doi.org/10.3978/j.issn.2218-676X.2014.10.01
125. Dimcevski G, Kotopoulis S, Bjånes T, Hoem D, Schjøtt J, Gjertsen BT et al (2016) A human clinical trial using ultrasound and microbubbles to enhance gemcitabine treatment of inoperable pancreatic cancer. J Control Release 243:172–181. https://doi.org/10.1016/j.jconrel.2016.10.007
126. Khokhlova TD, Haider Y, Hwang JH (2015) Therapeutic potential of ultrasound microbubbles in gastrointestinal oncology: recent advances and future prospects. Therap Adv Gastroenterol 8:384–394. https://doi.org/10.1177/1756283X15592584
127. Alexandrov AV, Molina CA, Grotta JC, Garami Z, Ford SR, Alvarez-Sabin J et al (2004) Ultrasound-enhanced systemic thrombolysis for acute ischemic stroke. N Engl J Med 351:2170–2178. https://doi.org/10.1056/NEJMoa041175
128. Hu J, Zhang N Jr, Li L, Zhang N Sr, Ma Y, Zhao C et al (2018) The synergistic bactericidal effect of vancomycin on UTMD treated biofilm involves damage to bacterial cells and enhancement of metabolic activities. Sci Rep 8:192. https://doi.org/10.1038/s41598-017-18496-3
129. Lattwein KR, Shekhar H, Kouijzer JJP, van Wamel WJB, Holland CK, Kooiman K (2020) Sonobactericide: an emerging treatment strategy for bacterial infections. Ultrasound Med Biol 46:193–215. https://doi.org/10.1016/j.ultrasmedbio.2019.09.011
130. Lattwein KR, Shekhar H, van Wamel WJB, Gonzalez T, Herr AB, Holland CK et al (2018) An in vitro proof-of-principle study of sonobactericide. Sci Rep 8:3411. https://doi.org/10.1038/s41598-018-21648-8
131. Dong Y, Li J, Li P, Yu J (2018) Ultrasound microbubbles enhance the activity of vancomycin against staphylococcus epidermidis biofilms in vivo. J Ultrasound Med 37:1379–1387. https://doi.org/10.1002/jum.14475
132. Zhu X, Guo J, He C, Geng H, Yu G, Li J et al (2016) Ultrasound triggered image-guided drug delivery to inhibit vascular reconstruction via paclitaxel-loaded microbubbles. Sci Rep 6:21683. https://doi.org/10.1038/srep21683
133. Kilroy JP, Dhanaliwala AH, Klibanov AL, Bowles DK, Wamhoff BR, Hossack JA (2015) Reducing neointima formation in a swine model with IVUS and sirolimus microbubbles. Ann Biomed Eng 43:2642–2651. https://doi.org/10.1007/s10439-015-1315-6
134. Nomikou N, Fowley C, Byrne NM, McCaughan B, McHale AP, Callan JF (2012) Microbubble-sonosensitiser conjugates as therapeutics in sonodynamic therapy. Chem Commun (Camb) 48:8332–8334. https://doi.org/10.1039/c2cc33913g
135. McEwan C, Fowley C, Nomikou N, McCaughan B, McHale AP, Callan JF (2014) Polymeric microbubbles as delivery vehicles for sensitizers in sonodynamic therapy. Langmuir 30:14926–14930. https://doi.org/10.1021/la503929c
136. Yang H, Sun Y, Wei J, Xu L, Tang Y, Yang L et al (2019) The effects of ultrasound-targeted microbubble destruction (UTMD) carrying IL-8 monoclonal antibody on the inflammatory responses and stability of atherosclerotic plaques. Biomed Pharmacother 118:109161. https://doi.org/10.1016/j.biopha.2019.109161
137. Horsley H, Owen J, Browning R, Carugo D, Malone-Lee J, Stride E et al (2019) Ultrasound-activated microbubbles as a novel intracellular drug delivery system for urinary tract infection. J Control Release 301:166–175. https://doi.org/10.1016/j.jconrel.2019.03.017
138. Un K, Kawakami S, Suzuki R, Maruyama K, Yamashita F, Hashida M (2011) Suppression of melanoma growth and metastasis by DNA vaccination using an ultrasound-responsive and mannose-modified gene carrier. Mol Pharm 8:543–554. https://doi.org/10.1021/mp100369n
139. Un K, Kawakami S, Suzuki R, Maruyama K, Yamashita F, Hashida M (2010) Development of an ultrasound-responsive and mannose-modified gene carrier for DNA vaccine therapy. Biomaterials 31:7813–7826. https://doi.org/10.1016/j.biomaterials.2010.06.058
140. Dewitte H, Van Lint S, Heirman C, Thielemans K, De Smedt SC, Breckpot K et al (2014) The potential of antigen and TriMix sonoporation using mRNA-loaded microbubbles for ultrasound-triggered cancer immunotherapy. J Control Release 194:28–36. https://doi.org/10.1016/j.jconrel.2014.08.011
141. Lentacker I, De Geest BG, Vandenbroucke RE, Peeters L, Demeester J, De Smedt SC et al (2006) Ultrasound-responsive polymer-coated microbubbles that bind and protect DNA. Langmuir 22:7273–7278. https://doi.org/10.1021/la0603828
142. Geis NA, Mayer CR, Kroll RD, Hardt SE, Katus HA, Bekeredjian R (2009) Spatial distribution of ultrasound targeted microbubble destruction increases cardiac transgene expression but not capillary permeability. Ultrasound Med Biol 35:1119–1126. https://doi.org/10.1016/j.ultrasmedbio.2009.01.008
143. Bekeredjian R, Kroll RD, Fein E, Tinkov S, Coester C, Winter G et al (2007) Ultrasound targeted microbubble destruction increases capillary permeability in hepatomas. Ultrasound Med Biol 33:1592–1598. https://doi.org/10.1016/j.ultrasmedbio.2007.05.003
144. Liu H, Chang S, Sun J, Zhu S, Pu C, Zhu Y et al (2014) Ultrasound-mediated destruction of LHRHa-targeted and paclitaxel-loaded lipid microbubbles induces proliferation inhibition and

apoptosis in ovarian cancer cells. Mol Pharm 11:40–48. https://doi.org/10.1021/mp4005244
145. Yan F, Li X, Jin Q, Jiang C, Zhang Z, Ling T et al (2011) Therapeutic ultrasonic microbubbles carrying paclitaxel and LyP-1 peptide: preparation, characterization and application to ultrasound-assisted chemotherapy in breast cancer cells. Ultrasound Med Biol 37:768–779. https://doi.org/10.1016/j.ultrasmedbio.2011.02.006
146. Zhou Y, Gu H, Xu Y, Li F, Kuang S, Wang Z et al (2015) Targeted antiangiogenesis gene therapy using targeted cationic microbubbles conjugated with CD105 antibody compared with untargeted cationic and neutral microbubbles. Theranostics 5:399–417. https://doi.org/10.7150/thno.10351
147. Crake C, Owen J, Smart S, Coviello C, Coussios CC, Carlisle R et al (2016) Enhancement and passive acoustic mapping of cavitation from fluorescently tagged magnetic resonance-visible magnetic microbubbles in vivo. Ultrasound Med Biol 42:3022–3036. https://doi.org/10.1016/j.ultrasmedbio.2016.08.002
148. Chertok B, Langer R (2018) Circulating magnetic microbubbles for localized real-time control of drug delivery by ultrasonography-guided magnetic targeting and ultrasound. Theranostics 8:341–357. https://doi.org/10.7150/thno.20781
149. Beguin E, Bau L, Shrivastava S, Stride E (2019) Comparing strategies for magnetic functionalization of microbubbles. ACS Appl Mater Interfaces 11:1829–1840. https://doi.org/10.1021/acsami.8b18418
150. Hynynen K, McDannold N, Sheikov NA, Jolesz FA, Vykhodtseva N (2005) Local and reversible blood-brain barrier disruption by noninvasive focused ultrasound at frequencies suitable for trans-skull sonications. Neuroimage 24:12–20. https://doi.org/10.1016/j.neuroimage.2004.06.046
151. Hynynen K, McDannold N, Martin H, Jolesz FA, Vykhodtseva N (2003) The threshold for brain damage in rabbits induced by bursts of ultrasound in the presence of an ultrasound contrast agent (Optison). Ultrasound Med Biol 29:473–481. https://doi.org/10.1016/s0301-5629(02)00741-x
152. McDannold N, Vykhodtseva N, Raymond S, Jolesz FA, Hynynen K (2005) MRI-guided targeted blood-brain barrier disruption with focused ultrasound: histological findings in rabbits. Ultrasound Med Biol 31:1527–1537. https://doi.org/10.1016/j.ultrasmedbio.2005.07.010
153. Liu HL, Wai YY, Chen WS, Chen JC, Hsu PH, Wu XY et al (2008) Hemorrhage detection during focused-ultrasound induced blood-brain-barrier opening by using susceptibility-weighted magnetic resonance imaging. Ultrasound Med Biol 34:598–606. https://doi.org/10.1016/j.ultrasmedbio.2008.01.011
154. Fan CH, Liu HL, Huang CY, Ma YJ, Yen TC, Yeh CK (2012) Detection of intracerebral hemorrhage and transient blood-supply shortage in focused-ultrasound-induced blood-brain barrier disruption by ultrasound imaging. Ultrasound Med Biol 38:1372–1382. https://doi.org/10.1016/j.ultrasmedbio.2012.03.013
155. Wei KC, Chu PC, Wang HY, Huang CY, Chen PY, Tsai HC et al (2013) Focused ultrasound-induced blood-brain barrier opening to enhance temozolomide delivery for glioblastoma treatment: a preclinical study. PLoS ONE 8:e58995. https://doi.org/10.1371/journal.pone.0058995
156. Liu HL, Huang CY, Chen JY, Wang HY, Chen PY, Wei KC (2014) Pharmacodynamic and therapeutic investigation of focused ultrasound-induced blood-brain barrier opening for enhanced temozolomide delivery in glioma treatment. PLoS ONE 9:e114311. https://doi.org/10.1371/journal.pone.0114311
157. Liu HL, Hua MY, Chen PY, Chu PC, Pan CH, Yang HW et al (2010) Blood-brain barrier disruption with focused ultrasound enhances delivery of chemotherapeutic drugs for glioblastoma treatment. Radiology 255:415–425. https://doi.org/10.1148/radiol.10090699
158. Treat LH, McDannold N, Vykhodtseva N, Zhang Y, Tam K, Hynynen K (2007) Targeted delivery of doxorubicin to the rat brain at therapeutic levels using MRI-guided focused ultrasound. Int J Cancer 121:901–907. https://doi.org/10.1002/ijc.22732
159. Beccaria K, Canney M, Goldwirt L, Fernandez C, Piquet J, Perier MC et al (2016) Ultrasound-induced opening of the blood-brain barrier to enhance temozolomide and irinotecan delivery: an experimental study in rabbits. J Neurosurg 124:1602–1610. https://doi.org/10.3171/2015.4.Jns142893
160. Zhang DY, Dmello C, Chen L, Arrieta VA, Gonzalez-Buendia E, Kane JR et al (2020) Ultrasound-mediated delivery of paclitaxel for glioma: a comparative study of distribution, toxicity, and efficacy of albumin-bound versus cremophor formulations. Clin Cancer Res 26:477–486. https://doi.org/10.1158/1078-0432.Ccr-19-2182
161. Treat LH, McDannold N, Zhang Y, Vykhodtseva N, Hynynen K (2012) Improved anti-tumor effect of liposomal doxorubicin after targeted blood-brain barrier disruption by MRI-guided focused ultrasound in rat glioma. Ultrasound Med Biol 38:1716–1725. https://doi.org/10.1016/j.ultrasmedbio.2012.04.015
162. Aryal M, Vykhodtseva N, Zhang YZ, McDannold N (2015) Multiple sessions of liposomal doxorubicin delivery via focused ultrasound mediated blood-brain barrier disruption: a safety study. J Control Release 204:60–69. https://doi.org/10.1016/j.jconrel.2015.02.033
163. Sun T, Zhang YZ, Power C, Alexander PM, Sutton JT, Aryal M et al (2017) Closed-loop control of targeted ultrasound drug delivery across the blood-brain/tumor barriers in a rat glioma model. Proc Natl Acad Sci USA 114:E10281–E10290. https://doi.org/10.1073/pnas.1713328114
164. McDannold N, Zhang YZ, Supko JG, Power C, Sun T, Peng CG et al (2019) Acoustic feedback enables safe and reliable carboplatin delivery across the blood-brain barrier with a clinical focused ultrasound system and improves survival in a rat glioma model. Theranostics 9:6284–6299. https://doi.org/10.7150/thno.35892
165. Chen PY, Hsieh HY, Huang CY, Lin CY, Wei KC, Liu HL (2015) Focused ultrasound-induced blood-brain barrier opening to enhance interleukin-12 delivery for brain tumor immunotherapy: a preclinical feasibility study. J Transl Med 13:93. https://doi.org/10.1186/s12967-015-0451-y
166. Kinoshita M, McDannold N, Jolesz FA, Hynynen K (2006) Noninvasive localized delivery of Herceptin to the mouse brain by MRI-guided focused ultrasound-induced blood-brain barrier disruption. Proc Natl Acad Sci U S A 103:11719–11723. https://doi.org/10.1073/pnas.0604318103
167. Kinoshita M, McDannold N, Jolesz FA, Hynynen K (2006) Targeted delivery of antibodies through the blood-brain barrier by MRI-guided focused ultrasound. Biochem Biophys Res Commun 340:1085–1090. https://doi.org/10.1016/j.bbrc.2005.12.112
168. Liu HL, Hsu PH, Lin CY, Huang CW, Chai WY, Chu PC et al (2016) Focused ultrasound enhances central nervous system delivery of bevacizumab for malignant glioma treatment. Radiology 281:99–108. https://doi.org/10.1148/radiol.2016152444
169. Park EJ, Zhang YZ, Vykhodtseva N, McDannold N (2012) Ultrasound-mediated blood-brain/blood-tumor barrier disruption improves outcomes with trastuzumab in a breast cancer brain metastasis model. J Control Release 163:277–284. https://doi.org/10.1016/j.jconrel.2012.09.007
170. Carpentier A, Canney M, Vignot A, Reina V, Beccaria K, Horodyckid C et al (2016) Clinical trial of blood-brain barrier disruption by pulsed ultrasound. Sci Transl Med 8:343re342. https://doi.org/10.1126/scitranslmed.aaf6086
171. Idbaih A, Canney M, Belin L, Desseaux C, Vignot A, Bouchoux G et al (2019) Safety and feasibility of repeated and transient blood-brain barrier disruption by pulsed ultrasound in patients

with recurrent glioblastoma. Clin Cancer Res 25:3793–3801. https://doi.org/10.1158/1078-0432.CCR-18-3643
172. Raymond SB, Treat LH, Dewey JD, McDannold NJ, Hynynen K, Bacskai BJ (2008) Ultrasound enhanced delivery of molecular imaging and therapeutic agents in Alzheimer's disease mouse models. PLoS ONE 3:e2175. https://doi.org/10.1371/journal.pone.0002175
173. Jordao JF, Ayala-Grosso CA, Markham K, Huang Y, Chopra R, McLaurin J et al (2010) Antibodies targeted to the brain with image-guided focused ultrasound reduces amyloid-beta plaque load in the TgCRND8 mouse model of Alzheimer's disease. PLoS ONE 5:e10549. https://doi.org/10.1371/journal.pone.0010549
174. Burgess A, Dubey S, Yeung S, Hough O, Eterman N, Aubert I et al (2014) Alzheimer disease in a mouse model: MR imaging-guided focused ultrasound targeted to the hippocampus opens the blood-brain barrier and improves pathologic abnormalities and behavior. Radiology 273:736–745. https://doi.org/10.1148/radiol.14140245
175. Nisbet RM, Van der Jeugd A, Leinenga G, Evans HT, Janowicz PW, Gotz J (2017) Combined effects of scanning ultrasound and a tau-specific single chain antibody in a tau transgenic mouse model. Brain 140:1220–1230. https://doi.org/10.1093/brain/awx052
176. Dubey S, Heinen S, Krantic S, McLaurin J, Branch DR, Hynynen K et al (2020) Clinically approved IVIg delivered to the hippocampus with focused ultrasound promotes neurogenesis in a model of Alzheimer's disease. Proc Natl Acad Sci USA 117:32691–32700. https://doi.org/10.1073/pnas.1908658117
177. Leinenga G, Gotz J (2015) Scanning ultrasound removes amyloid-beta and restores memory in an Alzheimer's disease mouse model. Sci Transl Med 7:278ra233. https://doi.org/10.1126/scitranslmed.aaa2512
178. Meng Y, Shirzadi Z, MacIntosh B, Heyn C, Smith GS, Aubert I et al (2019) Blood-brain barrier opening in alzheimer's disease using mr-guided focused ultrasound. Neurosurgery 66:65–65
179. Meng Y, MacIntosh BJ, Shirzadi Z, Kiss A, Bethune A, Heyn C et al (2019) Resting state functional connectivity changes after MR-guided focused ultrasound mediated blood-brain barrier opening in patients with Alzheimer's disease. Neuroimage 200:275–280. https://doi.org/10.1016/j.neuroimage.2019.06.060
180. Burgess A, Huang Y, Querbes W, Sah DW, Hynynen K (2012) Focused ultrasound for targeted delivery of siRNA and efficient knockdown of Htt expression. J Control Release 163:125–129. https://doi.org/10.1016/j.jconrel.2012.08.012
181. Hsu PH, Wei KC, Huang CY, Wen CJ, Yen TC, Liu CL et al (2013) Noninvasive and targeted gene delivery into the brain using microbubble-facilitated focused ultrasound. PLoS ONE 8:e57682. https://doi.org/10.1371/journal.pone.0057682
182. Noroozian Z, Xhima K, Huang Y, Kaspar BK, Kugler S, Hynynen K et al (2019) MRI-guided focused ultrasound for targeted delivery of rAAV to the brain. Methods Mol Biol 1950:177–197. https://doi.org/10.1007/978-1-4939-9139-6_10
183. Lin CY, Hsieh HY, Pitt WG, Huang CY, Tseng IC, Yeh CK et al (2015) Focused ultrasound-induced blood-brain barrier opening for non-viral, non-invasive, and targeted gene delivery. J Control Release 212:1–9. https://doi.org/10.1016/j.jconrel.2015.06.010
184. Fan CH, Ting CY, Lin CY, Chan HL, Chang YC, Chen YY et al (2016) Noninvasive, targeted, and non-viral ultrasound-mediated GDNF-plasmid delivery for treatment of Parkinson's disease. Sci Rep 6:19579. https://doi.org/10.1038/srep19579
185. Lin CY, Hsieh HY, Chen CM, Wu SR, Tsai CH, Huang CY et al (2016) Non-invasive, neuron-specific gene therapy by focused ultrasound-induced blood-brain barrier opening in Parkinson's disease mouse model. J Control Release 235:72–81. https://doi.org/10.1016/j.jconrel.2016.05.052
186. Long L, Cai XD, Guo RM, Wang P, Wu LL, Yin TH et al (2017) Treatment of Parkinson's disease in rats by Nrf2 transfection using MRI-guided focused ultrasound delivery of nanomicrobubbles. Biochem Biophys Res Commun 482:75–80. https://doi.org/10.1016/j.bbrc.2016.10.141
187. Gasca-Salas C, Fernandez-Rodriguez B, Pineda-Pardo JA, Rodriguez-Rojas R, Hernandez F, Obeso I et al (2020) Blood-brain barrier opening with focused ultrasound in Parkinson's disease dementia: a safety and feasibility study. Neurology 94(15)
188. Gasca-Salas C, Fernandez-Rodriguez B, Pineda-Pardo JA, Rodriguez-Rojas R, Obeso I, Hernandez-Fernandez F et al (2021) Blood-brain barrier opening with focused ultrasound in Parkinson's disease dementia. Nature Commun. https://doi.org/10.1038/s41467-021-21022-9
189. McDannold N, Zhang YZ, Power C, Arvanitis CD, Vykhodtseva N, Livingstone M (2015) Targeted, noninvasive blockade of cortical neuronal activity. Sci Rep. https://doi.org/10.1038/srep16253
190. Chu PC, Liu HL, Lai HY, Lin CY, Tsai HC, Pei YC (2015) Neuromodulation accompanying focused ultrasound-induced blood-brain barrier opening. Sci Rep 5:15477. https://doi.org/10.1038/srep15477
191. Todd N, Zhang YZ, Arcaro M, Becerr L, Borsook D, Livingstone M et al (2018) Focused ultrasound induced opening of the blood-brain barrier disrupts inter-hemispheric resting state functional connectivity in the rat brain. Neuroimage 178:414–422. https://doi.org/10.1016/j.neuroimage.2018.05.063
192. Cui ZW, Li DP, Feng Y, Xu TQ, Wu S, Li YB et al (2019) Enhanced neuronal activity in mouse motor cortex with microbubbles' oscillations by transcranial focused ultrasound stimulation. Ultrason Sonochem. https://doi.org/10.1016/j.ultsonch.2019.104745
193. Todd N, Zhang Y, Power C, Becerra L, Borsook D, Livingstone M et al (2019) Modulation of brain function by targeted delivery of GABA through the disrupted blood-brain barrier. Neuroimage 189:267–275. https://doi.org/10.1016/j.neuroimage.2019.01.037
194. Ibsen S, Tong A, Schutt C, Esener S, Chalasani SH (2015) Sonogenetics is a non-invasive approach to activating neurons in Caenorhabditis elegans. Nat Commun 6:8264. https://doi.org/10.1038/ncomms9264
195. Huang YS, Fan CH, Hsu N, Chiu NH, Wu CY, Chang CY et al (2020) Sonogenetic modulation of cellular activities using an engineered auditory-sensing protein. Nano Lett 20:1089–1100. https://doi.org/10.1021/acs.nanolett.9b04373
196. Kovacs ZI, Kim S, Jikaria N, Qureshi F, Milo B, Lewis BK et al (2017) Disrupting the blood-brain barrier by focused ultrasound induces sterile inflammation. Proc Natl Acad Sci U S A 114:E75–E84. https://doi.org/10.1073/pnas.1614777114
197. McMahon D, Bendayan R, Hynynen K (2017) Acute effects of focused ultrasound-induced increases in blood-brain barrier permeability on rat microvascular transcriptome. Sci Rep. https://doi.org/10.1038/srep45657
198. McMahon D, Hynynen K (2017) Acute inflammatory response following increased blood-brain barrier permeability induced by focused ultrasound is dependent on microbubble dose. Theranostics 7:3989–4000. https://doi.org/10.7150/thno.21630
199. Liu HL, Hsieh HY, Lu LA, Kang CW, Wu MF, Lin CY (2012) Low-pressure pulsed focused ultrasound with microbubbles promotes an anticancer immunological response. J Transl Med 10:221. https://doi.org/10.1186/1479-5876-10-221
200. Chen PY, Wei KC, Liu HL (2015) Neural immune modulation and immunotherapy assisted by focused ultrasound induced blood-brain barrier opening. Hum Vaccin Immunother 11:2682–2687. https://doi.org/10.1080/21645515.2015.1071749
201. Chen KT, Chai WY, Lin YJ, Lin CJ, Chen PY, Tsai HC et al (2021) Neuronavigation-guided focused ultrasound for

transcranial blood-brain barrier opening and immunostimulation in brain tumors. Sci Adv. https://doi.org/10.1126/sciadv.abd0772
202. Williams R, Wright C, Cherin E, Reznik N, Lee M, Gorelikov I et al (2013) Characterization of submicron phase-change perfluorocarbon droplets for extravascular ultrasound imaging of cancer. Ultrasound Med Biol 39:475–489. https://doi.org/10.1016/j.ultrasmedbio.2012.10.004
203. Phillips LC, Puett C, Sheeran PS, Wilson Miller G, Matsunaga TO, Dayton PA (2013) Phase-shift perfluorocarbon agents enhance high intensity focused ultrasound thermal delivery with reduced near-field heating. J Acoust Soc Am 134:1473–1482. https://doi.org/10.1121/1.4812866
204. Rapoport N, Gao Z, Kennedy A (2007) Multifunctional nanoparticles for combining ultrasonic tumor imaging and targeted chemotherapy. J Natl Cancer Inst 99:1095–1106. https://doi.org/10.1093/jnci/djm043
205. Zhang G, Harput S, Lin ST, Christensen-Jeffries K, Leow CH, Brown J et al (2018) Acoustic wave sparsely activated localization microscopy (AWSALM): Super-resolution ultrasound imaging using acoustic activation and deactivation of nanodroplets. Appl Phys Lett. https://doi.org/10.1063/1.5029874
206. Zhang G, Harput S, Hu H, Christensen-Jeffries K, Zhu J, Brown J et al (2019) Fast acoustic wave sparsely activated localization microscopy (fast-AWSALM): ultrasound super-resolution using plane-wave activation of nanodroplets. IEEE Trans Ultrason Ferroelectr Freq Control. https://doi.org/10.1109/TUFFC.2019.2906496
207. Shpak O, Verweij M, de Jong N, Versluis M (2016) Droplets, bubbles and ultrasound interactions. Adv Exp Med Biol 880:157–174. https://doi.org/10.1007/978-3-319-22536-4_9
208. Wu Q, Mannaris C, May JP, Bau L, Polydorou A, Ferri S et al (2021) Investigation of the acoustic vaporization threshold of lipid-coated perfluorobutane nanodroplets using both high-speed optical imaging and acoustic methods. Ultrasound Med Biol. https://doi.org/10.1016/j.ultrasmedbio.2021.02.019
209. Wang CH, Kang ST, Lee YH, Luo YL, Huang YF, Yeh CK (2012) Aptamer-conjugated and drug-loaded acoustic droplets for ultrasound theranosis. Biomaterials 33:1939–1947. https://doi.org/10.1016/j.biomaterials.2011.11.036
210. Seda R, Li DS, Fowlkes JB, Bull JL (2015) Characterization of bioeffects on endothelial cells under acoustic droplet vaporization. Ultrasound Med Biol 41:3241–3252. https://doi.org/10.1016/j.ultrasmedbio.2015.07.019
211. Harmon JS, Kabinejadian F, Seda R, Fabiilli ML, Kuruvilla S, Kuo CC et al (2019) Minimally invasive gas embolization using acoustic droplet vaporization in a rodent model of hepatocellular carcinoma. Sci Rep. https://doi.org/10.1038/s41598-019-47309-y
212. Feng Y, Qin D, Zhang J, Zhang L, Bouakaz A, Wan MX (2018) Occlusion and rupture of ex vivo capillary bifurcation due to acoustic droplet vaporization. Appl Phys Lett. https://doi.org/10.1063/15025594
213. Kripfgans OD, Fabiilli ML, Carson PL, Fowlkes JB (2004) On the acoustic vaporization of micrometer-sized droplets. J Acoust Soc Am 116:272–281. https://doi.org/10.1121/1.1755236
214. Kang ST, Huang YL, Yeh CK (2014) Characterization of acoustic droplet vaporization for control of bubble generation under flow conditions. Ultrasound Med Biol 40:551–561. https://doi.org/10.1016/j.ultrasmedbio.2013.10.020
215. Rapoport NY, Kennedy AM, Shea JE, Scaife CL, Nam KH (2009) Controlled and targeted tumor chemotherapy by ultrasound-activated nanoemulsions/microbubbles. J Control Release 138:268–276. https://doi.org/10.1016/j.jconrel.2009.05.026
216. Airan RD, Meyer RA, Ellens NP, Rhodes KR, Farahani K, Pomper MG et al (2017) Noninvasive targeted transcranial neuromodulation via focused ultrasound gated drug release from nanoemulsions. Nano Lett 17:652–659. https://doi.org/10.1021/acs.nanolett.6b03517
217. Lea-Banks H, O'Reilly MA, Hamani C, Hynynen K (2020) Localized anesthesia of a specific brain region using ultrasound-responsive barbiturate nanodroplets. Theranostics 10:2849–2858. https://doi.org/10.7150/thno.41566
218. Fabiilli ML, Haworth KJ, Fakhri NH, Kripfgans OD, Carson PL, Fowlkes JB (2009) The role of inertial cavitation in acoustic droplet vaporization. IEEE Trans Ultrason Ferroelectr Freq Control 56:1006–1017. https://doi.org/10.1109/TUFFC.2009.1132
219. Lo AH, Kripfgans OD, Carson PL, Rothman ED, Fowlkes JB (2007) Acoustic droplet vaporization threshold: effects of pulse duration and contrast agent. IEEE Trans Ultrason Ferroelectr Freq Control 54:933–946. https://doi.org/10.1109/tuffc.2007.339
220. Sheeran PS, Matsunaga TO, Dayton PA (2013) Phase-transition thresholds and vaporization phenomena for ultrasound phase-change nanoemulsions assessed via high-speed optical microscopy. Phys Med Biol 58:4513–4534. https://doi.org/10.1088/0031-9155/58/13/4513
221. Sheeran PS, Yoo K, Williams R, Yin M, Foster FS, Burns PN (2016) More than bubbles: creating phase-shift droplets from commercially available ultrasound contrast agents. Ultrasound Med Biol 43:531–540. https://doi.org/10.1016/j.ultrasmedbio.2016.09.003
222. Sheeran PS, Luois S, Dayton PA, Matsunaga TO (2011) Formulation and acoustic studies of a new phase-shift agent for diagnostic and therapeutic ultrasound. Langmuir 27:10412–10420. https://doi.org/10.1021/la2013705
223. Sheeran PS, Wong VP, Luois S, McFarland RJ, Ross WD, Feingold S et al (2011) Decafluorobutane as a phase-change contrast agent for low-energy extravascular ultrasonic imaging. Ultrasound Med Biol 37:1518–1530. https://doi.org/10.1016/j.ultrasmedbio.2011.05.021
224. Sheeran PS, Luois SH, Mullin LB, Matsunaga TO, Dayton PA (2012) Design of ultrasonically-activatable nanoparticles using low boiling point perfluorocarbons. Biomaterials 33:3262–3269. https://doi.org/10.1016/j.biomaterials.2012.01.021
225. Fan CH, Lin YT, Ho YJ, Yeh CK (2018) Spatial-temporal cellular bioeffects from acoustic droplet vaporization. Theranostics 8:5731–5743. https://doi.org/10.7150/thno.28782
226. Kang ST, Yeh CK (2011) Intracellular acoustic droplet vaporization in a single peritoneal macrophage for drug delivery applications. Langmuir 27:13183–13188. https://doi.org/10.1021/la203212p
227. Fan CH, Lee YH, Ho YJ, Wang CH, Kang ST, Yeh CK (2018) Macrophages as drug delivery carriers for acoustic phase-change droplets. Ultrasound Med Biol 44:1468–1481. https://doi.org/10.1016/j.ultrasmedbio.2018.03.009
228. Gorelikov I, Martin AL, Seo M, Matsuura N (2011) Silica-coated quantum dots for optical evaluation of perfluorocarbon droplet interactions with cells. Langmuir 27:15024–15033. https://doi.org/10.1021/la202679p
229. Ho YJ, Chiang YJ, Kang ST, Fan CH, Yeh CK (2018) Camptothecin-loaded fusogenic nanodroplets as ultrasound theranostic agent in stem cell-mediated drug-delivery system. J Control Release 278:100–109. https://doi.org/10.1016/j.jconrel.2018.04.001
230. Samuel S, Duprey A, Fabiilli ML, Bull JL, Fowlkes JB (2012) In vivo microscopy of targeted vessel occlusion employing acoustic droplet vaporization. Microcirculation 19:501–509. https://doi.org/10.1111/j.1549-8719.2012.00176.x
231. Sontum P, Kvale S, Healey AJ, Skurtveit R, Watanabe R, Matsumura M et al (2015) Acoustic cluster therapy (ACT)–A novel concept for ultrasound mediated, targeted drug delivery. Int J Pharm 495:1019–1027. https://doi.org/10.1016/j.ijpharm.2015.09.047

232. Kripfgans OD, Orifici CM, Carson PL, Ives KA, Eldevik OP, Fowlkes JB (2005) Acoustic droplet vaporization for temporal and spatial control of tissue occlusion: a kidney study. IEEE Trans Ultrason Ferroelectr Freq Control 52:1101–1110. https://doi.org/10.1109/tuffc.2005.1503996
233. Ho YJ, Chang YC, Yeh CK (2016) Improving nanoparticle penetration in tumors by vascular disruption with acoustic droplet vaporization. Theranostics 6:392–403. https://doi.org/10.7150/thno.13727
234. Fang J, Nakamura H, Maeda H (2011) The EPR effect: Unique features of tumor blood vessels for drug delivery, factors involved, and limitations and augmentation of the effect. Adv Drug Deliv Rev 63:136–151. https://doi.org/10.1016/j.addr.2010.04.009
235. Rapoport N, Kennedy AM, Shea JE, Scaife CL, Nam KH (2010) Ultrasonic nanotherapy of pancreatic cancer: lessons from ultrasound imaging. Mol Pharm 7:22–31. https://doi.org/10.1021/mp900128x
236. Rapoport N, Nam KH, Gupta R, Gao Z, Mohan P, Payne A et al (2011) Ultrasound-mediated tumor imaging and nanotherapy using drug loaded, block copolymer stabilized perfluorocarbon nanoemulsions. J Control Release 153:4–15. https://doi.org/10.1016/j.jconrel.2011.01.022
237. Helfield BL, Yoo K, Liu J, Williams R, Sheeran PS, Goertz DE et al (2020) Investigating the accumulation of submicron phase-change droplets in tumors. Ultrasound Med Biol 46:2861–2870. https://doi.org/10.1016/j.ultrasmedbio.2020.06.021
238. Lea-Banks H, Meng Y, Wu SK, Belhadjhamida R, Hamani C, Hynynen K (2021) Ultrasound-sensitive nanodroplets achieve targeted neuromodulation. J Control Release 332:30–39. https://doi.org/10.1016/j.jconrel.2021.02.010
239. Hu YX, Xue S, Long T, Lyu P, Zhang XY, Chen JQ et al (2020) Opto-acoustic synergistic irradiation for vaporization of natural melanin-cored nanodroplets at safe energy levels and efficient sono-chemo-photothermal cancer therapy. Theranostics 10:10448–10465. https://doi.org/10.7150/thno.44879
240. Mountford PA, Thomas AN, Borden MA (2015) Thermal activation of superheated lipid-coated perfluorocarbon drops. Langmuir 31:4627–4634. https://doi.org/10.1021/acs.langmuir.5b00399
241. Hannah AS, Luke GP, Emelianov SY (2016) Blinking phase-change nanocapsules enable background-free ultrasound imaging. Theranostics 6:1866–1876. https://doi.org/10.7150/thno.14961
242. Hallam KA, Donnelly EM, Karpiouk AB, Hartman RK, Emelianov SY (2018) Laser-activated perfluorocarbon nanodroplets: a new tool for blood brain barrier opening. Biomed Opt Express 9:4527–4538. https://doi.org/10.1364/BOE.9.004527
243. Harmon JS, Celingant-Copie CA, Kabinejadian F, Bull JL (2020) Lipid shell retention and selective binding capability following repeated transient acoustic microdroplet vaporization. Langmuir 36:6626–6634. https://doi.org/10.1021/acs.langmuir.0c00320
244. Aliabouzar M, Kripfgans OD, Wang WY, Baker BM, Brian Fowlkes J, Fabiilli ML (2021) Stable and transient bubble formation in acoustically-responsive scaffolds by acoustic droplet vaporization: theory and application in sequential release. Ultrason Sonochem 72:105430. https://doi.org/10.1016/j.ultsonch.2020.105430
245. Fan CH, Wang TW, Hsieh YK, Wang CF, Gao Z, Kim A et al (2019) Enhancing boron uptake in brain glioma by a boron-polymer/microbubble complex with focused ultrasound. ACS Appl Mater Interfaces 11:11144–11156. https://doi.org/10.1021/acsami.8b22468
246. Cai X, Jiang Y, Lin M, Zhang J, Guo H, Yang F et al (2019) Ultrasound-responsive materials for drug/gene delivery. Front Pharmacol 10:1650. https://doi.org/10.3389/fphar.2019.01650